International Journal of Solids and Structures 204–205 (2020) 138–152

Contents lists available at ScienceDirect

International Journal of Solids and Structures

journal homepage: www.elsevier.com/locate/ijsolstr

Wave attenuation in elastic metamaterial thick plates: Analytical, numerical and experimental investigations

E.J.P. Miranda Jr. [a,b,*], E.D. Nobrega [c], S.F. Rodrigues [b], C. Aranas Jr. [d], J.M.C. Dos Santos [e]

[a] Federal Institute of Maranhão, IFMA-EIB-DE, Rua Afonso Pena, 174, CEP 65010-030 São Luís, MA, Brazil
[b] Federal Institute of Maranhão, IFMA-PPGEM, Avenida Getúlio Vargas, 4, CEP 65030-005 São Luís, MA, Brazil
[c] Federal University of Maranhão, UFMA-CCET-CCEM, Avenida dos Portugueses, 1966, CEP 65080-805 São Luís, MA, Brazil
[d] University of New Brunswick, Department of Mechanical Engineering, Fredericton E3B 5A3, New Brunswick, Canada
[e] University of Campinas, UNICAMP-FEM-DMC, Rua Mendeleyev, 200, CEP 13083-970 Campinas, SP, Brazil

ARTICLE INFO

Article history:
Received 6 March 2020
Received in revised form 12 July 2020
Accepted 3 August 2020
Available online 19 August 2020

Keywords:
Metamaterial thick plate
Mindlin-Reissner theory
3D printing
Complex band structure
Forced response
Plane wave expansion

ABSTRACT

We investigate the complex band structure and forced response of flexural waves propagating in an elastic metamaterial thick plate. Mindlin-Reissner thick plate theory is considered. We study the influence of periodic arrays of spring-mass resonators attached to the surface of a homogeneous thick plate on the formation of Bragg-type and locally resonant band gaps. The plane wave expansion and extended plane wave expansion approaches are used to compute the complex band structure and wave shapes of the metamaterial thick plate with attached spring-mass resonators. An experimental analysis is conducted with a 3D-printed metamaterial plate with resonators. Modal shapes, forced response and band structure are computed by finite element and wave finite element methods. Analytical, numerical and experimental results present good agreement.

1. Introduction

Plate structures are widely used in aeronautical, mechanical and civil engineering, aerospace, manufacturing etc. They are one of the most commonly used structural components (Caliri et al., 2016; Li et al., 2019). Because of their many resonances, plates are mechanically soft and their suspending structures have considerable effect on their vibration and sound radiation (Hannon, 1975). The properties of a plate structure facilitate the generation of typically unwanted vibration radiation noise, which limits its practical application (Li et al., 2019). The noise and vibration are common phenomena in engineering and cause high-precision system malfunctions and extensive sound environment pollution (Huang et al., 2018). Thus, in order to control the vibration of plate structures, the strategy of using periodic systems has been proposed to create band gaps (Wang et al., 2019; He et al., 2017; Liu et al., 2018; Li et al., 2020b; Carta et al., 2020; Dal Poggetto and Arruda, 2021). These periodic structures are known as phononic crystals (PnCs) (Sigalas and Economou, 1992; Kushwaha et al., 1994; Liu and Gao, 2007; Pennec et al., 2010; Zhang and Gao, 2018; Dal Poggetto and Arruda, 2021) and mechanical metamaterials (MMs) (Liu et al., 2000; Bertoldi et al., 2017; Yu et al., 2018; Surjadi et al., 2019).

PnCs and MMs have been applied to vibration control (Casadei et al., 2012; Gao et al., 2016a; Gao et al., 2016b; Krushynska et al., 2017a; Li et al., 2017; Chen et al., 2017a; Sugino et al., 2018; Jung et al., 2019; Kamotski and Smyshlyaev, 2019; Zhang et al., 2020; Li et al., 2020a; Dal Poggetto and Serpa, 2020), as acoustic barriers (Ho et al., 2003; Yang et al., 2010; Liu et al., 2018), as noise suppression devices (Casadei et al., 2010; Xiao et al., 2012a) and to mechanical wave manipulation, *e.g.*, guiding, focusing, imaging, cloaking, and topological insulation (Lu et al., 2009; Maldovan, 2013; Hussein et al., 2014; Lee et al., 2016; Morvaridi et al., 2018; Bao and Wang, 2019; Zhang et al., 2020). PnCs are typically composed by periodic arrays of inclusions embedded in a matrix. They have received renewed attention (Yu et al., 2013; Gao et al., 2015; Miranda Jr. and Dos Santos, 2017; Chen et al., 2017b; Xie et al., 2017; Qian and Shi, 2017; Bilal et al., 2017; Hedayatrasa et al., 2018; Yu et al., 2017; Miranda Jr. and Dos Santos, 2018) because they exhibit Bragg-type band gaps where there are no mechanical propagating waves, only evanescent waves. This type of band gap is opened up because of the Bragg scattering. However, the Bragg scattering mechanism fails to open up band gaps in low frequencies for periodic structures with a small lattice parameter.

* Corresponding author at:Federal Institute of Maranhão, IFMA-EIB-DE, Rua Afonso Pena, 174, CEP 65010-030 São Luís, MA, Brazil.
E-mail address: edson.jansen@ifma.edu.br (E.J.P. Miranda Jr.).

https://doi.org/10.1016/j.ijsolstr.2020.08.002
0020-7683/

Difficulties to design PnCs with low frequency band gaps and small size stimulated researchers to explore the local resonance mechanism (Liu et al., 2000), *i.e.*, creating the MMs, also known as locally resonant PnCs.

According to Jung et al. (2019), focusing on noise and vibration applications, MMs can be classified into locally resonant metamaterial (Liu et al., 2000), acoustic black hole (Deng et al., 2019), membrane-type acoustic metamaterial (Lu et al., 2020) and metaporous (Yang et al., 2015). There are also the laminate MMs (Qian and Shi, 2016; He et al., 2017; Zuo et al., 2018). This investigation focus on locally resonant metamaterial thick plates, named elastic metamaterial (EM) thick plates, also known as platonic crystals (McPhedran et al., 2018; Movchan et al., 2018).

EMs can produce both locally resonant and Bragg-type band gaps. However, EMs just present Bragg-type band gaps if the system is periodic. Locally resonant band gaps arise in the vicinity of the natural frequency of the resonator while Bragg-type band gaps typically occur at wave lengths of the order of unit cell size. There are various types of EMs being investigated containing arrays of spring-mass resonators, such as rods (Wang et al., 2005a; Xiao et al., 2012b; Nobrega et al., 2016; Lou et al., 2018, beams (Wang et al., 2005b; Yu et al., 2006a; Yu et al., 2006b; Liu et al., 2007; Xiao et al., 2012c; Raghavan and Phani, 2013; Wang and Wang, 2013; Wang et al., 2013; Xiao et al., 2013; Casadei and Bertoldi, 2014; Wang et al., 2015; Wang et al., 2016; Sugino et al., 2017; Cheng et al., 2018; Miranda Jr. and Dos Santos, 2019; Wu et al., 2019; Li et al., 2020a, plates (Sun et al., 2010; Oudich et al., 2011; Xiao et al., 2012d; Claeys et al., 2013; Torrent et al., 2013; Oudich et al., 2014; Chen et al., 2014; Peng et al., 2015; Song et al., 2015; Chen et al., 2017a; Lu et al., 2017; Pal and Ruzzene, 2017; Haslinger et al., 2017; Sugino et al., 2017; He et al., 2017; Sugino et al., 2018; Miranda Jr. et al., 2019; Wang et al., 2019; Xiao et al., 2019; Li et al., 2020b; Carta et al., 2020) and shells (Thorp et al., 2005). We consider an EM thick plate with periodic arrays of spring-mass resonators. Mindlin-Reissner thick plate theory (Mindlin, 1951) is regarded. We highlight that only few studies used thick plate theory for EM plate modelling with resonators (Hsu and Wu, 2010; Oudich et al., 2014; Assouar et al., 2016; Beli et al., 2018a; Wu et al., 2018; Li et al., 2019), since it is more complex mathematically.

Oudich and co-workers (Oudich et al., 2014) studied the sound transmission loss performance through an EM thick plate made of spring-mass resonators attached to the surface of a homogeneous elastic plate. However, instead of considering flexural waves using Mindlin-Reissner thick plate, they regarded a solid media (from which all the Lamb modes are taken into consideration) using the plane wave expansion (PWE) approach associated with the supercell technique (Han and Zhang, 2019). They reported that high sound transmission loss up to 72 dB at 2 kHz is reached with an EM thick plate while only 23 dB can be obtained for a simple homogeneous plate with the same thickness. Wu et al. (2018) investigated the influence of thermal stresses on the band structure of EM thick plates by using the finite element (FE) based method. The resonator was not modelled by spring-mass and they regarded single and double inclusions of square plates. They observed that thermal stresses have a nonlinear effect on the band structures, which is significant and cannot be ignored when EM thick plates are embedded in thermal environments. Li et al. (2019) studied a complete low-frequency band gap in a thick elastic steel metamaterial plate. The resonator-type structure consists of periodic, double-sided, composite stepped resonators, which are deposited on the EM thick plate. They used the FE method for band structure, power-transmission spectra, and displacement fields of the eigenmodes calculations. They showed that, for the proposed structure, the opening of the first complete band gap is reduced by a factor of 9.5 compared to a conventional thick elastic steel metamaterial plate.

Since periodic resonator-type structures attached to thick plates started recently to be studied in many engineering applications for vibration management (Hsu and Wu, 2010; Oudich et al., 2014; Assouar et al., 2016; Achaoui et al., 2013; Beli et al., 2018a; Li et al., 2019), the main purpose of this study is to investigate the complex band structure of flexural waves propagating in an EM thick plate with multiple single degree of freedom (S-DOF) resonators. To the best of our knowledge, this is the first study to consider an EM thick plate with attached multiple spring-mass resonators using the Mindlin-Reissner (Mindlin, 1951) theory. We think it is worth using thick plate theory, since the S-DOF resonators can be tuned at high frequencies (Qian, 2020), where the traditional thin plate theory, *i.e.*, Kirchhoff–Love plate theory (Kirchhoff, 1850; Love, 1888), is not valid. Moreover, PWE (Sigalas and Economou, 1992; Kushwaha et al., 1994) and extended plane wave expansion (EPWE) (Hsue and Yang, 2004a; Hsue and Yang, 2004b; Hsue and Freeman, 2005; Laude et al., 2009; Romero-García et al., 2010a; Romero-García et al., 2010b; Romero-García et al., 2010c) methods are used for the first time to predict the complex band structure and wave shapes of an EM thick plate with spring-mass resonators regarding Mindlin-Reissner theory (Mindlin, 1951). These approaches can predict more accurate results at higher frequencies than previous formulations (Xiao et al., 2012d; Torrent et al., 2013; Xiao et al., 2014; Sugino et al., 2017; Zuo et al., 2018; Miranda Jr. et al., 2019; Wang et al., 2019; Sugino et al., 2020) based on Kirchhoff–Love thin plate theory (Kirchhoff, 1850; Love, 1888).

By using a 3D-printed EM plate, an experimental test is performed. An EM plate with square lattice is manufactured with a polymer (Vero White Plus) in a 3D printer with UV curing technology. Simulated results with FE, wave finite element (WFE), PWE and EPWE are compared to the experimental data. Some mismatches between simulated and experimental results are found. These differences are reduced after a trial-and-error model updating by varying material property parameters (Young's modulus and mass density). PWE and EPWE modelling with spring-mass S-DOF resonators localize band gap position and width close to the experimental results and also close to the FE and WFE results with the 3D resonators.

The paper is organized as follows. Section 2 presents fundamentals of PWE and EPWE approaches for an EM thick plate with periodic arrays of attached resonators based on Mindlin-Reissener plate theory (Mindlin, 1951). In the following, *i.e.*, Section 3, simulated examples are carried out considering some test cases: (I) single resonator and (II) multiple resonators in the unit cell. In Section 4, an experimental validation of an EM plate and simulated verification using FE, WFE, PWE and EPWE are performed. Conclusions are presented in Section 5.

2. Elastic metamaterial thick plate modelling

This section presents the basic concepts of PWE and EPWE approaches for an EM thick plate based on Mindlin-Reissner plate theory (Mindlin, 1951). We consider two-dimensional periodicity, *i.e.*, 2D EM, isotropic elastic plate and wave propagation in the *xy* plane.

PWE and EPWE are semi-analytical methods used to calculate the band structure and wave shapes of PnCs and EMs. The advantage of using EPWE over PWE is that evanescent modes are obtained naturally, thus the complex band structure can be investigated. In PWE, it is assumed that the Bloch wave vector is real. In addition, using the EPWE method, the Bloch wave vector is not restricted to the first Brillouin (Brillouin, 1946) zone (FBZ) (Laude

et al., 2009). Hsue and co-workers (Hsue and Freeman, 2005) proved that the evanescent modes obtained by EPWE obey Floquet-Bloch's theorem (Floquet, 1883; Bloch, 1928).

There are some recent studies that have been developed for EM thin plate modelling using PWE and EPWE methods (Xiao et al., 2012d; Torrent et al., 2013; Xiao et al., 2014; Sugino et al., 2017; Zuo et al., 2018; Miranda Jr. et al., 2019; Wang et al., 2019; Sugino et al., 2020). Xiao and co-workers (Xiao et al., 2012d) proposed PWE and EPWE methods to model a metamaterial Kirchhoff–Love (Kirchhoff, 1850; Love, 1888) plate with attached resonators of S-DOF in the unit cell. Miranda Jr. et al. (2019) presented new formulations for PWE and EPWE approaches for an EM thin plate with periodic arrays of attached multiple degrees of freedom (M-DOF) resonators based on Kirchhoff–Love plate theory (Kirchhoff, 1850; Love, 1888). Moreover, Torrent and co-workers (Torrent et al., 2013) used the PWE method to study an EM thin plate with attached S-DOF resonators, considering honeycomb lattice. Here, we consider for the first time an EM thick plate with attached multiple resonators of S-DOF in the unit cell.

Fig. 1 sketches the unit cell of an EM thick plate with attached multiple resonators of S-DOF, considering square lattice. Fig. 1 also illustrates the first irreducible Brillouin zone (FIBZ) (Brillouin, 1946) in shaded region for square lattice. The FIBZ points in Fig. 1 are $\Gamma\ (0,0)$, X $(\pi/a,0)$ and M $(\pi/a,\pi/a)$, where a is the lattice parameter. Each resonator has a stiffness k_j and a mass m_j, where j is the index related to the jth resonator.

2.1. Plane wave expansion

From Mindlin-Reissner plate theory (Mindlin, 1951), the governing equations for flexural vibration of a uniform thick plate can be written as:

$$\alpha\frac{\partial\hat{\Psi}_x(\mathbf{r},t)}{\partial x}+\alpha\frac{\partial^2\hat{w}(\mathbf{r},t)}{\partial x^2}+\alpha\frac{\partial\hat{\Psi}_y(\mathbf{r},t)}{\partial y}+\alpha\frac{\partial^2\hat{w}(\mathbf{r},t)}{\partial y^2}-\tau\ddot{\hat{w}}(\mathbf{r},t)=-\hat{p}(\mathbf{r},t), \tag{1a}$$

$$D\frac{\partial^2\hat{\Psi}_x(\mathbf{r},t)}{\partial x^2}+\beta\frac{\partial^2\hat{\Psi}_y(\mathbf{r},t)}{\partial x\partial y}+\gamma\frac{\partial^2\hat{\Psi}_y(\mathbf{r},t)}{\partial y\partial x}+\gamma\frac{\partial^2\hat{\Psi}_x(\mathbf{r},t)}{\partial y^2}-\alpha\hat{\Psi}_x(\mathbf{r},t)-\alpha\frac{\partial\hat{w}(\mathbf{r},t)}{\partial x}=\delta\ddot{\hat{\Psi}}_x(\mathbf{r},t), \tag{1b}$$

$$\gamma\frac{\partial^2\hat{\Psi}_y(\mathbf{r},t)}{\partial x^2}+\gamma\frac{\partial^2\hat{\Psi}_x(\mathbf{r},t)}{\partial x\partial y}+D\frac{\partial^2\hat{\Psi}_y(\mathbf{r},t)}{\partial y^2}+\beta\frac{\partial^2\hat{\Psi}_x(\mathbf{r},t)}{\partial y\partial x}-\alpha\hat{\Psi}_y(\mathbf{r},t)-\alpha\frac{\partial\hat{w}(\mathbf{r},t)}{\partial y}=\delta\ddot{\hat{\Psi}}_y(\mathbf{r},t), \tag{1c}$$

where $\alpha=\kappa^2\mu h$, $\kappa^2=\pi^2/12$, μ is the shear modulus, h is the plate thickness, $\tau=\rho h$, ρ is the density, $D=Eh^3/12(1-\nu^2)$ is the bending stiffness, E is the Young's modulus, ν is the Poisson's ratio, $\beta=D\nu$, $\gamma=D(1-\nu)/2$, $\delta=\rho h^3/12$, $\hat{w}(\mathbf{r},t)$ is the transverse displacement, $\hat{\Psi}_x(\mathbf{r},t)$ is the rotation around the x direction, $\hat{\Psi}_y(\mathbf{r},t)$ is the rotation around the y direction, $\hat{p}(\mathbf{r},t)$ is the external distributed load, $\mathbf{r}=x\mathbf{e}_1+y\mathbf{e}_2$ $(x,y\in\mathbb{R})$ is the two-dimensional spatial vector (the system has translational symmetry in z direction, *i.e.*, $\mathbf{r}$ depends only on the x and y coordinates) and $\mathbf{e}_i(i=1,2)$ are the basis vectors in the real space.

Applying the temporal Fourier transform to Eqs. (1a)–(1c) and omitting frequency dependence, they produce:

$$\alpha\frac{\partial\Psi_x(\mathbf{r})}{\partial x}+\alpha\frac{\partial^2w(\mathbf{r})}{\partial x^2}+\alpha\frac{\partial\Psi_y(\mathbf{r})}{\partial y}+\alpha\frac{\partial^2w(\mathbf{r})}{\partial y^2}+\omega^2\tau w(\mathbf{r})=-p(\mathbf{r}), \tag{2a}$$

$$D\frac{\partial^2\Psi_x(\mathbf{r})}{\partial x^2}+\beta\frac{\partial^2\Psi_y(\mathbf{r})}{\partial x\partial y}+\gamma\frac{\partial^2\Psi_y(\mathbf{r})}{\partial y\partial x}+\gamma\frac{\partial^2\Psi_x(\mathbf{r})}{\partial y^2}-\alpha\Psi_x(\mathbf{r})-\alpha\frac{\partial w(\mathbf{r})}{\partial x}+\omega^2\delta\Psi_x(\mathbf{r})=0, \tag{2b}$$

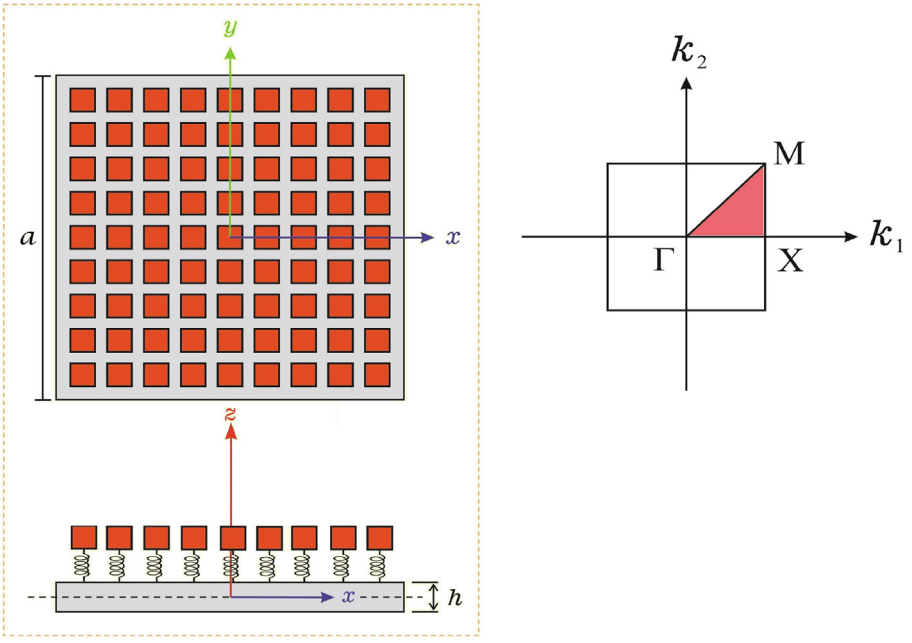

Fig. 1. Unit cell of the elastic metamaterial thick plate with attached multiple resonators of S-DOF for square lattice. First irreducible Brillouin zone in shaded region for a square lattice.

$$\gamma\frac{\partial^2\Psi_y(\mathbf{r})}{\partial x^2}+\gamma\frac{\partial^2\Psi_x(\mathbf{r})}{\partial x\partial y}+D\frac{\partial^2\Psi_y(\mathbf{r})}{\partial y^2}+\beta\frac{\partial^2\Psi_x(\mathbf{r})}{\partial y\partial x}-\alpha\Psi_y(\mathbf{r})-\alpha\frac{\partial w(\mathbf{r})}{\partial y}+\omega^2\delta\Psi_y(\mathbf{r})=0, \tag{2c}$$

where $w(\mathbf{r}), \Psi_x(\mathbf{r})$ and $\Psi_y(\mathbf{r})$ are the Fourier transforms of $\hat{w}(\mathbf{r},t), \hat{\Psi}_x(\mathbf{r},t)$ and $\hat{\Psi}_y(\mathbf{r},t)$.

Considering an EM thick plate with attached multiple resonators in the unit cell (Fig. 1), Eq. (2a) can be rewritten as,

$$\alpha\frac{\partial\Psi_x(\mathbf{r})}{\partial x}+\alpha\frac{\partial^2 w(\mathbf{r})}{\partial x^2}+\alpha\frac{\partial\Psi_y(\mathbf{r})}{\partial y}+\alpha\frac{\partial^2 w(\mathbf{r})}{\partial y^2}+\omega^2\tau w(\mathbf{r})=-\sum_{j=1}^{N}\sum_{\bar{\mathbf{r}}=-\infty}^{+\infty}p_j(\mathbf{r}_j+\bar{\mathbf{r}})\tilde{\delta}[\mathbf{r}-(\mathbf{r}_j+\bar{\mathbf{r}})], \tag{3}$$

where $\tilde{\delta}[\mathbf{r}-(\mathbf{r}_j+\bar{\mathbf{r}})]$ is the Dirac delta function, $p_j(\mathbf{r}_j+\bar{\mathbf{r}})$ is the force applied to the plate by the jth resonator and $\bar{\mathbf{r}}=\bar{p}\mathbf{a}_1+\bar{q}\mathbf{a}_2$ $(\bar{p},\bar{q}\in\mathbb{Z})$ is the lattice vector, $\mathbf{a}_i(i=1,2)$ are its vectorial components (also known as primitive vectors in real space). The primitive vectors for square lattice are given by $\mathbf{a}_i=a\mathbf{e}_i(i=1,2)$.

For attached multiple resonators of S-DOF, the $p_j(\mathbf{r}_j+\bar{\mathbf{r}})$ can be expressed by:

$$p_j(\mathbf{r}_j+\bar{\mathbf{r}})=k_j[u_j(\mathbf{r}_j+\bar{\mathbf{r}})-w(\mathbf{r}_j+\bar{\mathbf{r}})], \tag{4}$$

$$-\omega^2 m_j u_j(\mathbf{r}_j+\bar{\mathbf{r}})=-p_j(\mathbf{r}_j+\bar{\mathbf{r}}), \tag{5}$$

where $u_j(\mathbf{r}_j+\bar{\mathbf{r}})$ and $w(\mathbf{r}_j+\bar{\mathbf{r}})$ are the resonator and plate flexural displacements at position $\mathbf{r}_j+\bar{\mathbf{r}}$, respectively.

Due to the system periodicity, one can invoke the Floquet-Bloch's theorem (Floquet, 1883; Bloch, 1928):

$$H(\mathbf{r})=e^{i\mathbf{k}\cdot\mathbf{r}}H_{\mathbf{k}}(\mathbf{r}), \tag{6}$$

where H can be w, Ψ_x or Ψ_y and $H_{\mathbf{k}}(\mathbf{r})$ is the Bloch wave amplitude. Note that $H_{\mathbf{k}}(\mathbf{r})=H_{\mathbf{k}}(\mathbf{r}+\bar{\mathbf{r}})$ and $H(\mathbf{r}+\bar{\mathbf{r}})=H(\mathbf{r})e^{i\mathbf{k}\cdot\bar{\mathbf{r}}}$, where the exponential $e^{i\mathbf{k}\cdot\bar{\mathbf{r}}}$ is called Floquet-Bloch periodic boundary condition and $\mathbf{k}=\bar{u}\mathbf{b}_1+\bar{v}\mathbf{b}_2$ is the Bloch wave vector, where $(\bar{u},\bar{v}\in\mathbb{Q})$ are the symmetry points within the FIBZ in reciprocal space or we may write $\mathbf{k}=k_1\mathbf{e}_1+k_2\mathbf{e}_2$, where $(k_1,k_2\in\mathbb{R})$ are the point coordinates within the FIBZ for the reciprocal space, considering square lattice, *i.e.*, Fig. 1. The primitive vectors in reciprocal space, *i.e.*, $\mathbf{b}_i(i=1,2)$, are defined as $\mathbf{b}_1=2\pi\frac{\mathbf{a}_2\times\mathbf{a}_3}{\mathbf{a}_1\cdot(\mathbf{a}_2\times\mathbf{a}_3)}$ and $\mathbf{b}_2=2\pi\frac{\mathbf{a}_3\times\mathbf{a}_1}{\mathbf{a}_2\cdot(\mathbf{a}_3\times\mathbf{a}_1)}$. In addition, the primitive vectors in real and reciprocal spaces are related by $\mathbf{a}_i\cdot\mathbf{b}_j=2\pi\tilde{\delta}_{ij}, \tilde{\delta}_{ij}=0$ if $i\neq j$ or $\tilde{\delta}_{ij}=1$ if $i=j$ is the Kronecker delta.

Expanding $H_{\mathbf{k}}(\mathbf{r})$ in Fourier series in the reciprocal space, one can rewrite Eq. (6) as:

$$H(\mathbf{r})=e^{i\mathbf{k}\cdot\mathbf{r}}\sum_{\bar{\mathbf{g}}=-\infty}^{+\infty}H(\bar{\mathbf{g}})e^{i\bar{\mathbf{g}}\cdot\mathbf{r}}=\sum_{\bar{\mathbf{g}}=-\infty}^{+\infty}H(\bar{\mathbf{g}})e^{i(\mathbf{k}+\bar{\mathbf{g}})\cdot\mathbf{r}}, \tag{7}$$

where $\bar{\mathbf{g}}=\bar{m}\mathbf{b}_1+\bar{n}\mathbf{b}_2$ is the reciprocal lattice vector and it is regarded for square lattice, *i.e.*, $\bar{\mathbf{g}}=\frac{2\pi}{a}(\bar{m}\mathbf{e}_1+\bar{n}\mathbf{e}_2)$, with $(\bar{m},\bar{n}\in\mathbb{Z})$.

Similarly, applying Floquet-Bloch's theorem (Floquet, 1883; Bloch, 1928) and expanding in Fourier series in the reciprocal space, the variable $w(\mathbf{r}_j)$ can be written as:

$$w(\mathbf{r}_j)=\sum_{\tilde{\mathbf{g}}=-\infty}^{+\infty}w(\tilde{\mathbf{g}})e^{i(\mathbf{k}+\tilde{\mathbf{g}})\cdot\mathbf{r}_j}, \tag{8}$$

where $\tilde{\mathbf{g}}$ has the same expressions of $\bar{\mathbf{g}}$ for square lattice, with $(\tilde{m},\tilde{n}\in\mathbb{Z})$. From Floquet-Bloch periodic boundary condition, we can write $w(\mathbf{r}_j+\bar{\mathbf{r}})$ and $u_j(\mathbf{r}_j+\bar{\mathbf{r}})$ as:

$$w(\mathbf{r}_j+\bar{\mathbf{r}})=w(\mathbf{r}_j)e^{i\mathbf{k}\cdot\bar{\mathbf{r}}}, \tag{9}$$

$$u_j(\mathbf{r}_j+\bar{\mathbf{r}})=u_j(\mathbf{r}_j)e^{i\mathbf{k}\cdot\bar{\mathbf{r}}}. \tag{10}$$

Substituting Eqs. (7)–(10) in Eq. (3) and after some mathematical manipulations, one may write:

$$(\mathbf{K}-\omega^2\mathbf{M})\mathbf{q}=\mathbf{0}. \tag{11}$$

The mathematical details to obtain Eq. (11) and the expressions of matrices $\mathbf{K}$, $\mathbf{M}$ and vector $\mathbf{q}$ will be derived in a future publication. However, the procedure to obtain Eq. (11) is similar to that reported by (Xiao et al., 2012d; Miranda Jr. et al., 2019) for thin plates.

Eq. (11) represents a generalized eigenvalue problem of $\omega(\mathbf{k})$. This equation must be solved for each Bloch wave vector into the FIBZ, considering square lattice.

2.2. Extended plane wave expansion

The equation of motion of the jth resonator in Fig. 1 can be written as:

$$(\mathbf{K}_j-\omega^2\mathbf{M}_j)\mathbf{u}_j=\mathbf{p}_j, \tag{12}$$

with the stiffness matrix of the jth resonator given by:

$$\mathbf{K}_j=\begin{bmatrix}k_j & -k_j\\ -k_j & k_j\end{bmatrix}. \tag{13}$$

Assuming zero mass at the attachment point between the jth resonator and the EM thick plate, the mass matrix can be expressed as:

$$\mathbf{M}_j=\begin{bmatrix}0 & 0\\ 0 & m_j\end{bmatrix}. \tag{14}$$

The displacement vector of the metamaterial system is given by:

$$\mathbf{u}_j=\begin{Bmatrix}w(\mathbf{r}_j+\bar{\mathbf{r}})\\ u_j\end{Bmatrix}. \tag{15}$$

The force vector of the metamaterial system is given by:

$$\mathbf{p}_j=\begin{Bmatrix}-p_j(\mathbf{r}_j+\bar{\mathbf{r}})\\ p_j\end{Bmatrix}, \tag{16}$$

where $-p_j(\mathbf{r}_j+\bar{\mathbf{r}})$ is the plate reaction force at the attachment point.

Since there are no external forces acting on the resonator masses, *i.e.*, $p_j=0$, the metamaterial displacement vector can be condensed. Thus, Eq. (12) can be rewritten as:

$$p_j(\mathbf{r}_j+\bar{\mathbf{r}})=-D_j w(\mathbf{r}_j+\bar{\mathbf{r}}), \tag{17}$$

where D_j is the dynamic stiffness of the jth resonator given by:

$$D_j=\frac{-\omega^2 k_j m_j}{k_j-\omega^2 m_j}. \tag{18}$$

In order to include damping in the resonator, a complex stiffness is used, *i.e.*, $\tilde{k}_j=k_j(1+i\eta_j)$, where η_j is the damping of the jth resonator, also known as loss factor.

To obtain the EPWE formulation, Eq. (17) is substituted into the Eq. (3), producing:

$$\alpha\frac{\partial\Psi_x(\mathbf{r})}{\partial x}+\alpha\frac{\partial^2 w(\mathbf{r})}{\partial x^2}+\alpha\frac{\partial\Psi_y(\mathbf{r})}{\partial y}+\alpha\frac{\partial^2 w(\mathbf{r})}{\partial y^2}+\omega^2\tau w(\mathbf{r})-\sum_{j=1}^{N}\sum_{\bar{\mathbf{r}}=-\infty}^{+\infty}D_j w(\mathbf{r}_j+\bar{\mathbf{r}})\delta[\mathbf{r}-(\mathbf{r}_j+\bar{\mathbf{r}})]=0. \tag{19}$$

Inserting Eqs. (7)–(9) in Eqs. (19), (2b) and (2c) after some mathematical manipulations, one may write a standard eigenvalue problem:

$$\left(\begin{bmatrix}\mathbf{B}_1 & \mathbf{B}_2\\ \mathbf{0} & \mathbf{B}_1\end{bmatrix} - \bar{k}\begin{bmatrix}\mathbf{0} & -\mathbf{B}_3\\ \mathbf{B}_1 & \mathbf{0}\end{bmatrix}\right)\begin{Bmatrix}\bar{\mathbf{q}}\\ \bar{k}\bar{\mathbf{q}}\end{Bmatrix} = \begin{Bmatrix}\mathbf{0}\\ \mathbf{0}\end{Bmatrix}, \tag{20}$$

where $\bar{k} = ka$ and $k = \|\mathbf{k}\|$. The mathematical manipulations to produce Eq. (20) and the expressions of the sub-matrices $\mathbf{B}_1, \mathbf{B}_2, \mathbf{B}_3$ and vector $\bar{\mathbf{q}}$ will be derived in a future publication. However, the procedure to obtain Eq. (20) is similar to that reported by Xiao et al. (2012d) and Miranda Jr. et al. (2019) for thin plates.

Eq. (20) represents a generalized eigenvalue problem of $\mathbf{k}(\omega)$. The main advantage of EPWE as compared to PWE is to obtain the complex values of $\mathbf{k}$, which are related to the evanescent waves and attenuation of the unit cell, defined as $\tilde{\mu} = \Im\{\mathbf{k}\}a$.

3. Simulated examples

Simulated examples are performed in order to verify the PWE and EPWE methods with Mindlin-Reissner plate theory (Mindlin, 1951) and to demonstrate their capacity of calculating the complex band structure and wave shapes of an EM thick plate with attached multiple resonators of S-DOF.

For all examples, the EM thick plate geometry and material properties are shown in Table 1. They are chosen to be the same as used by Xiao et al. (2012d) and Miranda Jr. et al. (2019), in order to facilitate comparison.

A complex Young's modulus is regarded, *i.e.*, $\tilde{E} = E(1 + i\eta)$, with the purpose of including a structural damping in the EM thick plate.

We highlight that a criterion for tracking the frequency evolution of wave modes is used when EPWE is applied, similar to Miranda Jr. and Dos Santos (2019). In EPWE method, the wave modes are calculated at several discrete frequencies. Then, another issue is to associate, among all modes defined at a given frequency $(\omega + \Delta\omega)$, the one which matches a given mode defined at the previous frequency (ω).

We choose the model assurance criterion (MAC) to estimate the correlation among wave shapes. This criterion is based on the hermitian scalar product and it is useful for very low frequencies (Mencik, 2010). Given a wave shape l defined at an specific frequency ω and for a sufficiently small $\Delta\omega$, the wave shape l defined at frequency $\omega + \Delta\omega$ results in:

$$\left|\frac{\boldsymbol{\Phi}_l^H(\omega)}{\|\boldsymbol{\Phi}_l(\omega)\|}\frac{\boldsymbol{\Phi}_l(\omega+\Delta\omega)}{\|\boldsymbol{\Phi}_l(\omega+\Delta\omega)\|}\right| = max_s\left\{\left|\frac{\boldsymbol{\Phi}_l^H(\omega)}{\|\boldsymbol{\Phi}_l(\omega)\|}\frac{\boldsymbol{\Phi}_s(\omega+\Delta\omega)}{\|\boldsymbol{\Phi}_s(\omega+\Delta\omega)\|}\right|\right\}, \tag{21}$$

where $\|\boldsymbol{\Phi}_l\| = \sqrt{\boldsymbol{\Phi}_l^H\boldsymbol{\Phi}_l}$ denotes the hermitian norm of the eigenvectors $\boldsymbol{\Phi}_l$, which can be related to Eq. (20) by:

$$\boldsymbol{\Phi}_l = \begin{Bmatrix}\bar{\mathbf{q}}\\ \bar{k}\bar{\mathbf{q}}\end{Bmatrix}_l, \tag{22}$$

with $l, s = 1, \ldots, 6(2M+1)^2$, $(M \in \mathbb{Z})$, and $(\cdot)^H$ indicates the conjugate transpose. The complex band structures calculated by EPWE are ordered using MAC.

Table 1
Elastic metamaterial thick plate geometry and material properties.

Geometry/Property	Value
Lattice parameter (a)	0.1 m
Unit cell area ($S = a^2$)	0.01 m^2
Thickness (h)	0.002 m
Young's modulus (E)	70×10^9 Pa
Mass density (ρ)	2700 kg/m^3
Structural damping (η)	0.01
Poisson's ratio (ν)	0.3

For all PWE and EPWE calculations, 81 plane waves are used for Fourier series expansion. This resulted in a good convergence.

3.1. Single resonator of S-DOF – SRSD

We consider first an EM thick plate with an attached single resonator of S-DOF (SRSD) in the unit cell, as illustrated in Fig. 2. The S-DOF resonator parameters are $\eta_1 = 0.05, f_1 = 300$ Hz, $m_1 = \gamma_1\rho Sh$, where $\gamma_1 = 0.5$ is the ratio of resonator mass to the plate unit cell mass. The resonator stiffness is calculated by $k_1 = m_1(2\pi f_1)^2(1 + i\eta_1)$.

Fig. 3(a) shows the band structure real part of the EM thick plate proposed in this study calculated by PWE (blue asterisks). We plot the band structure real parts in the three principal symmetry directions of the FIBZ. The plots are given in terms of the real part of the reduced Bloch wave vector defined as $\mathbf{k}a/2\pi$ versus frequency in Hz. This band structure real part in Fig. 3(a) (blue asterisks) agrees with the results of Xiao et al. (2012d) and Miranda Jr. et al. (2019)(red circles), considering Kirchhoff–Love thin plate theory, *i.e.*, for lower frequencies, we observe a good agreement between thin and thick plate theories. However, for higher frequencies, Fig. 3(b), there is no agreement, since Kirchhoff–Love thin plate theory is not valid for higher frequencies. Kirchhoff–Love thin plate theory is only valid for $\|\mathbf{k}\|h \ll 1, h/a \ll 1$ (Yao et al., 2009) or $h < \lambda/6$ (Fahy and Gardonio, 2007). We do not consider a spring-mass S-DOF resonator with a high resonant frequency, however, we think it is worth using thick plate theory, since the resonators can be tuned at high frequencies (Qian, 2020), where the thin plate theory is not valid.

Moreover, in Fig. 3(a), one complete locally resonant band gap is found around the resonant frequency of 300 Hz (blue shaded region). Bragg-type band gaps are predicted by Bragg's law along different directions, *i.e.*, $a = n(\lambda/2\cos\phi),\ n \in \mathbb{Z}$. The first Bragg frequency along ΓX direction ($\phi = 0°$) is opened up around 484 Hz and this directional (partial) band gap can be observed in Fig. 3(a).

Fig. 4 illustrates the band structure imaginary parts calculated by EPWE for different directions inside FIBZ, regarding Kirchhoff–Love (Xiao et al., 2012d; Miranda Jr. et al., 2019) (a) and Mindlin-Reissner (b) plate theories. In Fig. 4(c), a good agreement is observed between both theories at lower frequencies even at the band gaps.

In Fig. 4, we consider only the smallest positive imaginary part of the reduced Bloch wave vector (lowest component whose real part of the reduced Bloch wave vector lies inside and around the FIBZ is the most accurate (Miranda Jr. and Dos Santos, 2019)), since it represents the least rapidly decaying wave (evanescent Bloch wave (Romero-García et al., 2010a; Romero-García et al., 2010b; Romero-García et al., 2010c)) that carries energy the farthest (Xiao et al., 2012d). Hereafter, only the smallest positive imaginary part of the reduced Bloch wave vector is considered in EPWE plots. From Fig. 4, the Bragg-type band gaps in different directions can be seen. Locally resonant band gaps vary slightly with ϕ. Moreover, the unit cell attenuation for locally resonant band gaps is higher than for Bragg-type band gaps.

In Fig. 5, we compute the wave shapes (associated with the locally resonant $(a-b)$ and Bragg-type $(c-d)$ band gaps) by Eq. (7), *i.e.*, $|w(\mathbf{r})|$, with $f_1 = 300$ Hz and the data of Table 1. We highlight that these wave shapes are associated only with the propagating modes of the band structure, since the values of $w(\bar{\mathbf{g}})$ in Eq. (7) are obtained from the eigenvectors of Eq. (11), $\mathbf{q}$, using PWE approach.

In Fig. 5($a-b$), we illustrate the wave shapes at the lower edge frequency (a) ($f = 270.3$ Hz, XM direction, at M) and at the upper edge frequency (b) ($f = 354.6$ Hz, MΓ direction, at Γ) of the locally resonant band gap. These wave shapes are related to the flexural

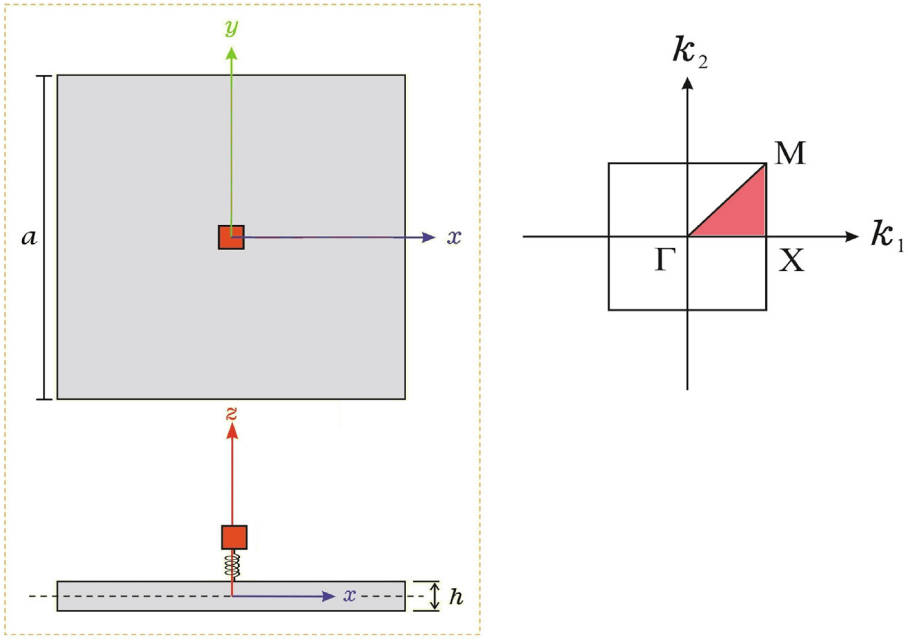

Fig. 2. Unit cell of the elastic metamaterial thick plate with attached single resonator of S-DOF for square lattice. First irreducible Brillouin zone in shaded region for a square lattice.

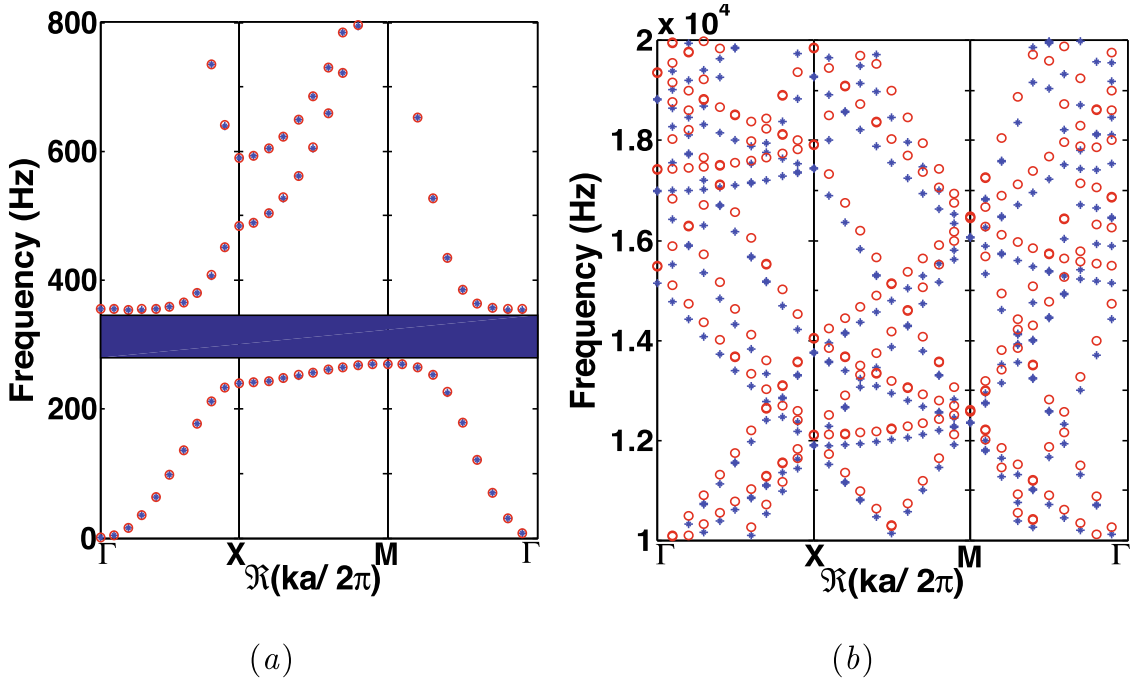

Fig. 3. Elastic band structure real parts of the EM plate considering thin plate theory (Kirchhoff–Love Xiao et al., 2012d; Miranda Jr. et al., 2019), red circles, and thick plate theory (Mindlin-Reissner), blue asterisks, for (a) lower and (b) higher frequencies, with $f_1 = 300$ Hz and the data of Table 1. (For interpretation of the references to color in this figure legend, the reader is referred to the web version of this article.)

modes of the EM thick plate whose vibrations are out-of-plane, *i.e.*, particles vibrate in the z-direction (perpendicular to the wave propagation). The wave shapes at lower and upper edge frequencies of the locally resonant band gap present similar pattern. The amplitudes of the displacement field in Fig. 5$(a-b)$ are confined in the unit cell and the interactions between displacement fields and their neighbours in adjacent unit cells are weak. The higher and lower amplitudes of $|w(\mathbf{r})|$ in Fig. 5$(a-b)$, respectively, are localized in the middle of the unit cell, at the same position of the attached resonator. We also highlight that a significant displacement is observed in Fig. 5(b) at the corners of the unit cell.

Fig. 5$(c-d)$ shows the wave shapes for $|w(\mathbf{r})|$ at the lower edge frequency (c) ($f = 483.7$ Hz, ΓX direction, at X) and at the upper edge frequency (d) ($f = 589.6$ Hz, ΓX direction, at X) of the first Bragg-type band gap. The amplitudes of the displacement field considering the first Bragg-type band gap (Fig. 5$(c-d)$) are lower than the amplitudes associated with the locally resonant band gap (Fig. 5$(a-b)$).

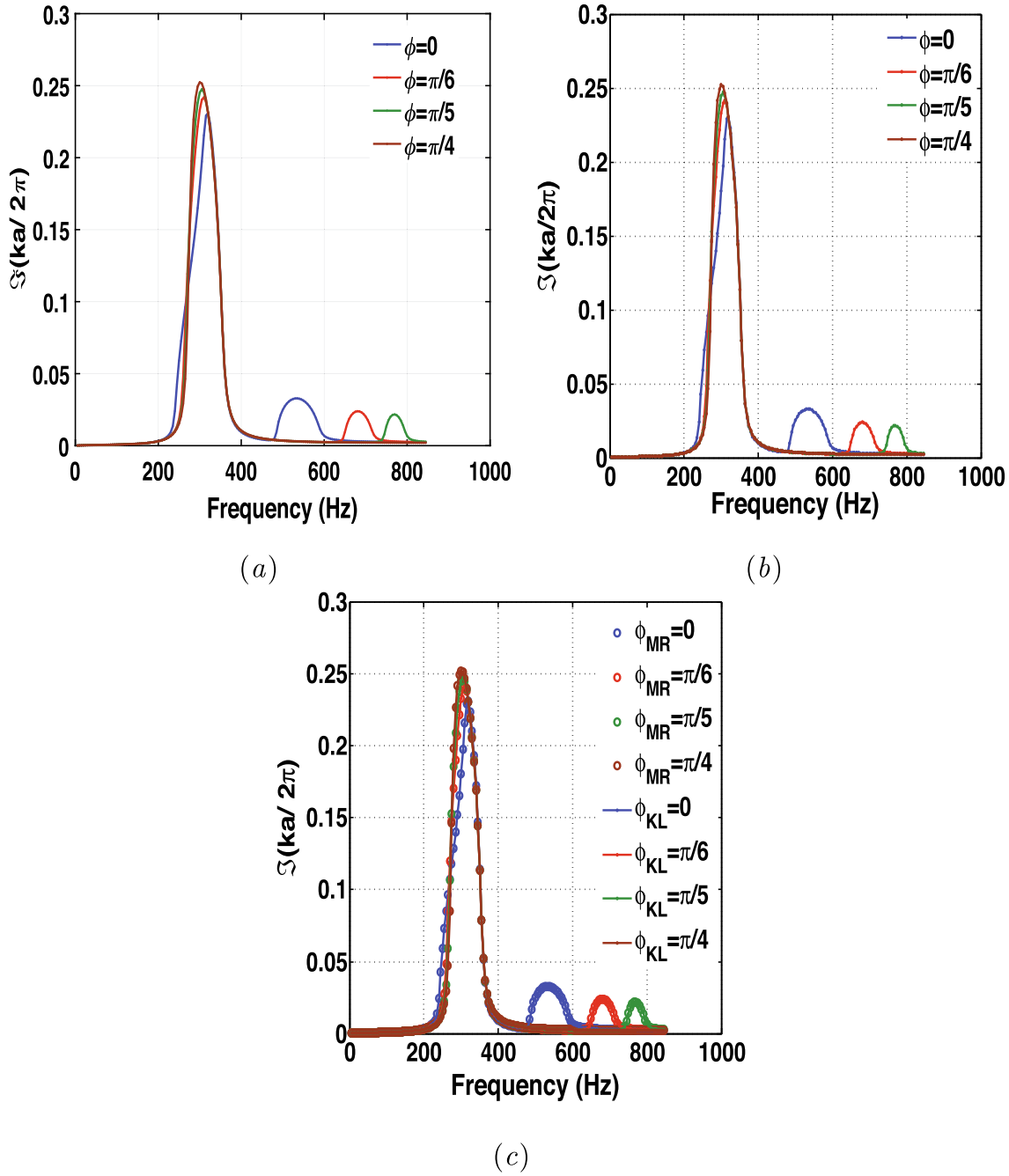

Fig. 4. Elastic band structure imaginary parts of the EM plate considering (a) thin plate theory (Kirchhoff–Love Xiao et al., 2012d; Miranda Jr. et al., 2019) and (b) thick plate theory (Mindlin-Reissner), with $f_1 = 300$ Hz and the data of Table 1, for different directions inside FIBZ. (c) Comparison of elastic band structure imaginary parts of the EM plate considering (a) thin plate theory (Kirchhoff–Love, KL, Xiao et al., 2012d; Miranda Jr. et al., 2019), dotted-line, and (b) thick plate theory (Mindlin-Reissner, MR), circles.

In Fig. 5$(c-d)$, the displacement field interacts mainly with their neighbours in adjacent unit cells at the two vertical boundaries with different intensities. The flexural waves could propagate freely between adjacent unit cells.

3.2. Multiple resonators of S-DOF – MRSD

In this subsection, we consider an EM thick plate with attached two resonators of S-DOF (MRSD) in the unit cell. The S-DOF resonator parameters are $f_j = \{283, 102\}$ Hz, $\gamma_j = 0.5 \times \{0.6, 0.4\}$, $m_j = \gamma_j \rho S h$, $\eta_j = 0.05$ and $k_j = m_j(2\pi f_j)^2 (1 + i\eta_j)$, where $j = 1, 2$. The sum of all ratio of resonator mass to the plate unit cell mass is equal to 0.5, the same as SRSD configuration.

Fig. 6 shows the band structure real part of the EM thick plate with attached double resonators of S-DOF in the unit cell. It can be seen the locally resonant band gaps near the natural frequencies of the resonators (283 Hz and 102 Hz). The resonator with natural frequency of 283 Hz opens up the broadest complete locally resonant band gap.

Fig. 7 illustrates the band structure imaginary part of the EM thick plate with attached double periodic arrays of S-DOF resonators. It can be seen the unit cell attenuation performance of the two locally resonant and the Bragg-type band gaps for different directions. The highest attenuation is associated with the natural

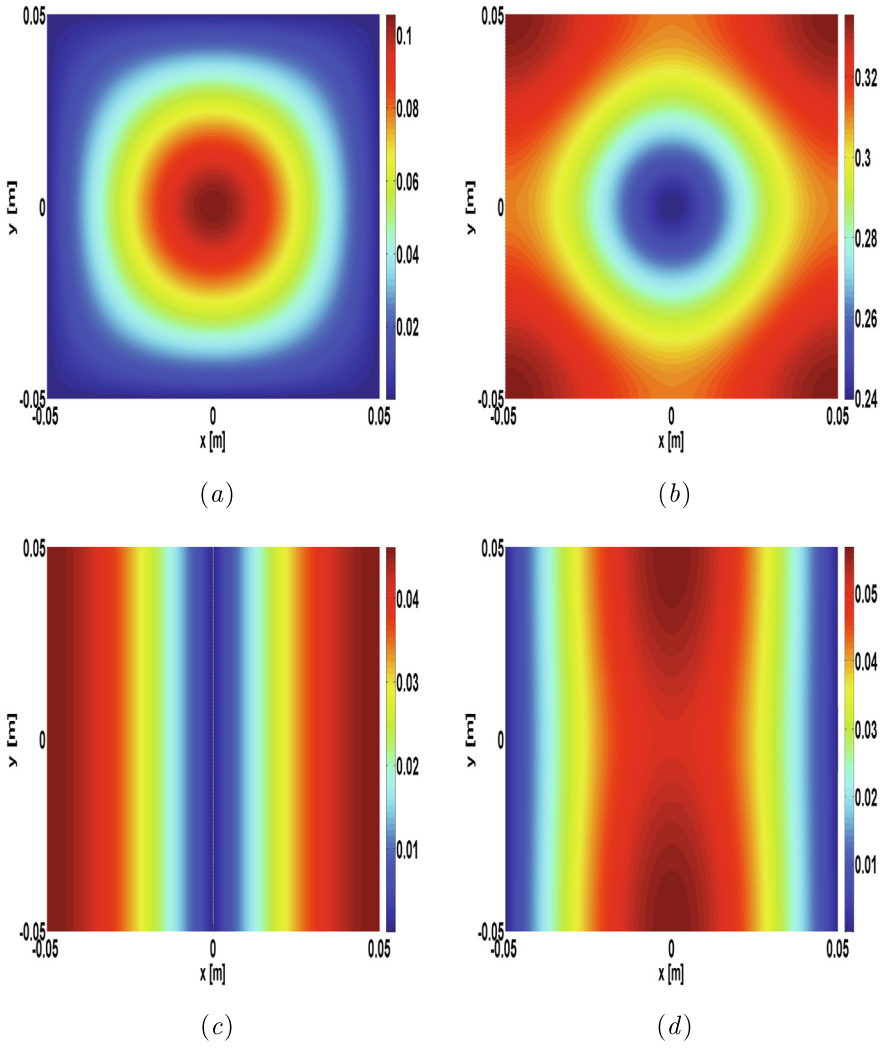

Fig. 5. Wave shapes ($|w(\mathbf{r})|$) computed by Eq. (7) for the EM thick plate at the (a) lower edge frequency ($f = 270.3$Hz, XM direction, at M), (b) upper edge frequency ($f = 354.6$ Hz, MΓ direction, at Γ) of the locally resonant band gap, (c) lower edge frequency ($f = 483.7$ Hz, ΓX direction, at X) and (d) upper edge frequency ($f = 589.6$ Hz, ΓX direction, at X) of the first Bragg-type band gap, considering $f_1 = 300$ Hz and the data of Table 1.

frequency of 283 Hz. One can note that the locally resonant and Bragg-type band gaps for SRSD configuration (Fig. 4) presents higher attenuation and are broader than the band gaps for MRSD configuration (Fig. 7).

In Fig. 8, we compute the wave shapes (related to the first $(a-b)$ and second $(c-d)$ locally resonant band gaps) by Eq. (7), *i.e.*, $|w(\mathbf{r})|$, with $f_j = \{283, 102\}$ Hz and the data of Table 1. These wave shapes are associated only with the propagating modes of the band structure. In Fig. 8$(a-b)$, we illustrate the wave shapes at the lower edge frequency (a) ($f = 101.3$ Hz, XM direction, at M) and at the upper edge frequency (b) ($f = 109.1$ Hz, MΓ direction, at Γ) of the first locally resonant band gap. Moreover, Fig. 8$(c-d)$ show the wave shapes at the lower edge frequency (c) ($f = 267.2$ Hz, XM direction, at M) and at the upper edge frequency (d) ($f = 317.2$ Hz, MΓ direction, at Γ) of the second locally resonant band gap.

The higher amplitudes in Fig. 8(a,c) and lower amplitudes in Fig. 8(b,d) of the displacement field are localized at the same position of the attached resonators, since the resonators are theoretically attached in the middle of the unit cell. Note that a significant displacement is observed in Fig. 8(b,d) at the corners of the unit cell, similar to the SRSD configuration (Fig. 5(b)).

The pattern of the wave shapes for both first (Fig. 8$(a-b)$) and second (Fig. 8$(c-d)$) locally resonant band gaps is similar. However, the amplitudes are higher for the wave shapes associated with the second locally resonant band gap (Fig. 8$(c-d)$). Moreover, the wave shapes associated with the locally resonant band gaps for MRSD (Fig. 8) present lower amplitudes than SRSD (Fig. 5).

Fig. 9 illustrates the wave shapes for $|w(\mathbf{r})|$ at the lower edge frequency (a) ($f = 483.7$ Hz, ΓX direction, at X) and at the upper edge frequency (b) ($f = 548.7$ Hz, ΓX direction, at X) of the first Bragg-type band gap.

The amplitudes of the displacement field considering the first Bragg-type band gap (Fig. 9) are lower than the amplitudes associated with the first and second locally resonant band gaps (Fig. 8), except for the lower edge frequency of the first locally resonant band gap (Fig. 8(a)).

The pattern of the wave shapes regarding the first Bragg-type band gap for MRSD (Fig. 9) is similar to the SRSD (Fig. 5). However, the amplitudes of the displacement field are higher for the SRSD,

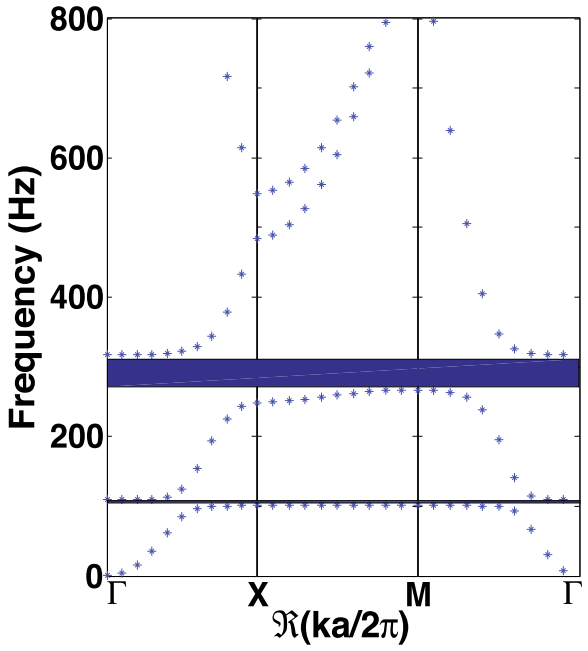

Fig. 6. Elastic band structure real part of EM thick plate with attached double periodic arrays of S-DOF resonators considering $f_j = \{283, 102\}$ Hz and the data of Table 1.

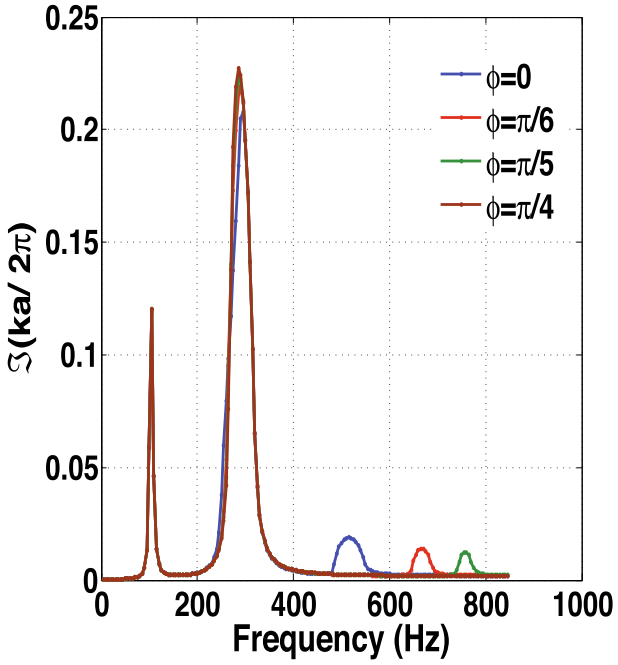

Fig. 7. Elastic band structure imaginary parts of the EM thick plate with attached double periodic arrays of S-DOF resonators considering $f_j = \{283, 102\}$ Hz and the data of Table 1, for different directions inside FIBZ.

considering the upper edge frequency (Fig. 5(*d*)), and for the MRSD, regarding the lower edge frequency (Fig. 9(*a*)).

4. Experimental validation and numerical verification

In this section, frequency response functions (FRFs) are computed for an EM plate and a comparison with the complex band structures is provided in order to identify the locally resonant band gaps. This comparison between finite (FRF) and infinite (band structure) metamaterials has been well addressed (Matlack et al., 2016; Hu et al., 2017; Krushynska et al., 2017b; Sugino et al., 2017; Ampatzidis et al., 2018; Zouari et al., 2018).

The EM plate was designed to be used as a metamaterial plate-like (flexural waves) structure with spatial periodic distribution and local resonators. Each unit cell contains one resonator consisting of a mass (0.006 m × 0.006 m × 0.0038 m) and a beam (0.001 m × 0.001 m × 0.002 m) on middle of unit cell that links the mass to the plate. The models of the unit cell, slice (for WFE modelling) and EM plate are shown in Fig. 10.

The EM plate (0.12 m × 0.096 m × 0.0028 m) was fabricated in a 3D printer. For the manufacture of the EM plate, the material was considered to be as isotropic as possible. However, this hypothesis is not necessarily fulfilled for additive manufacturing (Wang et al., 2017; Dizona et al., 2018; Ngo et al., 2018). Based on this requirement the EM plate was manufactured with plastic material (Vero White Plus) in a 3D printer with UV curing technology. Fig. 11 illustrates the EM plate and the experimental setup. The EM plate contains 10 × 8 resonators. An impact hammer excitation was used and the acceleration was obtained by a piezoelectric accelerometer.

The measurement instruments used in the experimental setup, Fig. 11, are summarized in Table 2.

The EM plate geometric parameters and material properties are summarized in Table 3. The material properties, *i.e.*, E, ρ and ν, were taken from manufacturer and adjusted in order to numerical results match the experimental results.

The modal analysis and forced response of the EM plate are computed with a commercial finite element analysis software ANSYS (Mechanical APDL Release 14.5). The EM plate is modelled using a 3D solid element (SOLID187). The global system is modelled using a free mesh with 12156 3D triangular elements. The boundary conditions of the EM plate are free edges. Furthermore, we also calculate the forced response using the WFE approach with the data obtained by ANSYS, *i.e.*, the same data of FE method.

Fig. 12 illustrates the mode shapes of the unit cell with a boundary condition of clamped on all edges (CCCC) computed by FE. We illustrate only the first three mode shapes of the unit cell at (*a*) 915.222 Hz, (*b*) 917.343 Hz and (*c*) 1075.14 Hz. These resonant frequencies are associated with the locally resonant band gap opened up for the EM plate. However, only the first two symmetry modes are the most important in this study, since only flexural waves are being considered for forced response calculation of the EM plate. Thus, for a hammer excitation as illustrated in Fig. 11, only the first two modes in Fig. 12 are important for the locally resonant band gap formation.

The numerical forced response of the EM plate is calculated considering the FE and WFE modelling described before. We also compute the experimental FRF of the 3D-printed EM plate with the LMS SCADAS data acquisition system. Fig. 13 compares the experimental (EXP) receptance FRF (*i.e.*, displacement divided by force) and receptance FRFs computed by FE and WFE approaches.

Fig. 13 illustrates that the locally resonant band gap calculated by FE and WFE is opened up between 870 Hz and 986 Hz, whereas for the experimental results the higher attenuation is observed from 630 Hz to 924 Hz. The FE and WFE results are in a very good agreement. We remark that numerical and experimental receptances present good agreement, but there is some mismatch. This issue should be associated with the uncertainty of the material properties (E and ρ) specified by the plastic manufacturer, which is not guaranteed in the addictive manufacturing process used to print the EM plate. Additive manufacturing, like any other manufacturing process, can introduce material and geometrical variabilities that affect the structural dynamic behaviour (Beli et al., 2019;

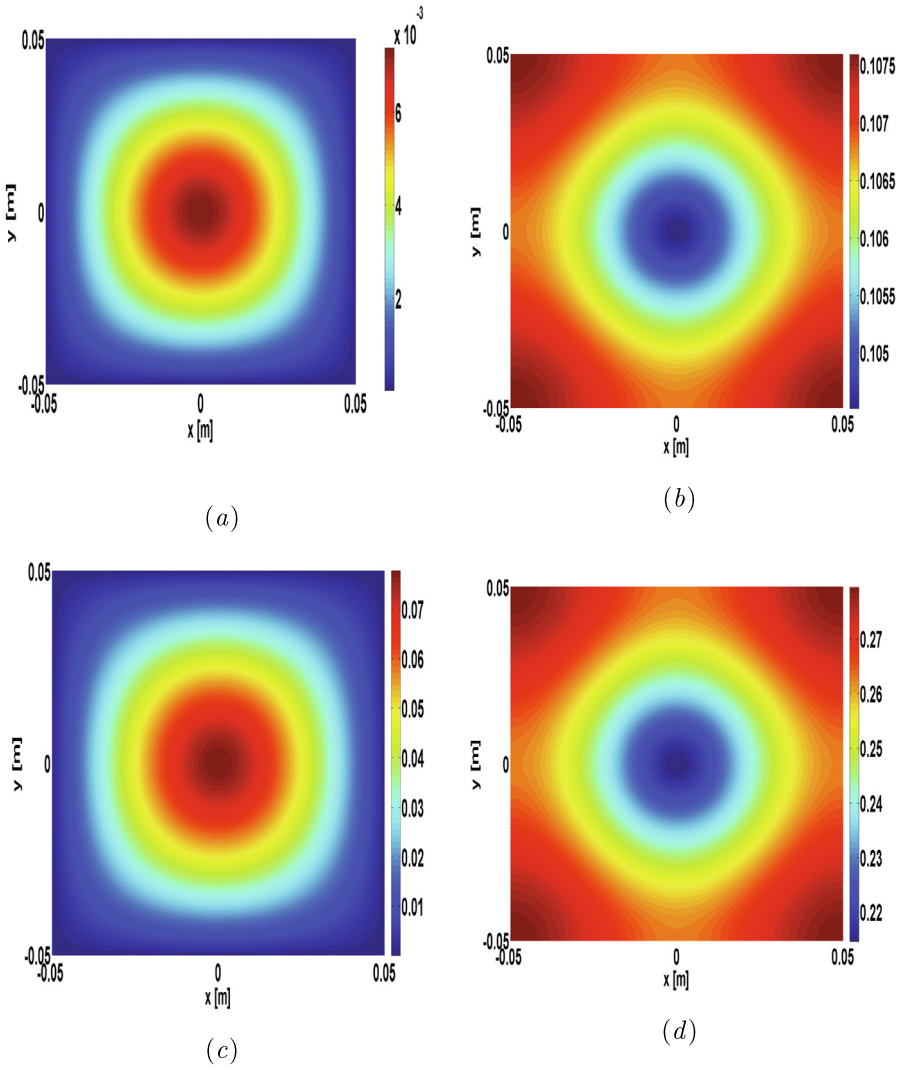

Fig. 8. Wave shapes ($|w(\mathbf{r})|$) computed by Eq. (7) for the EM thick plate at the (a) lower edge frequency ($f = 101.3$Hz, XM direction, at M), (b) upper edge frequency ($f = 109.1$ Hz, MΓ direction, at Γ) of the first locally resonant band gap, at the (c) lower edge frequency ($f = 267.2$ Hz, XM direction, at M) and (d) upper edge frequency ($f = 317.2$ Hz, MΓ direction, at Γ) of the second locally resonant band gap, considering $f_j = \{283, 102\}$ Hz and the data of Table 1.

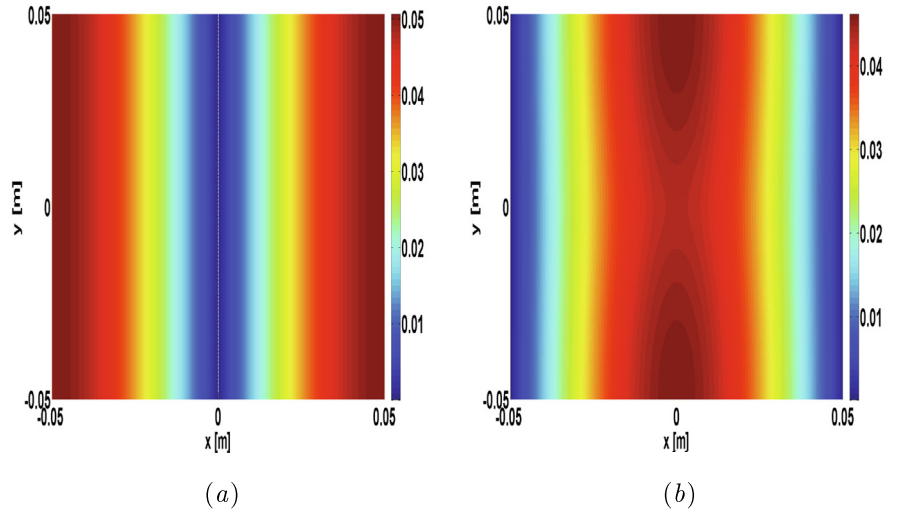

Fig. 9. Wave shapes ($|w(\mathbf{r})|$) computed by Eq. (7) for the EM thick plate at the (a) lower edge frequency ($f = 483.7$ Hz, ΓX direction, at X) and (b) upper edge frequency ($f = 548.7$ Hz, ΓX direction, at X) of the first Bragg-type band gap, considering $f_j = \{283, 102\}$ Hz and the data of Table 1.

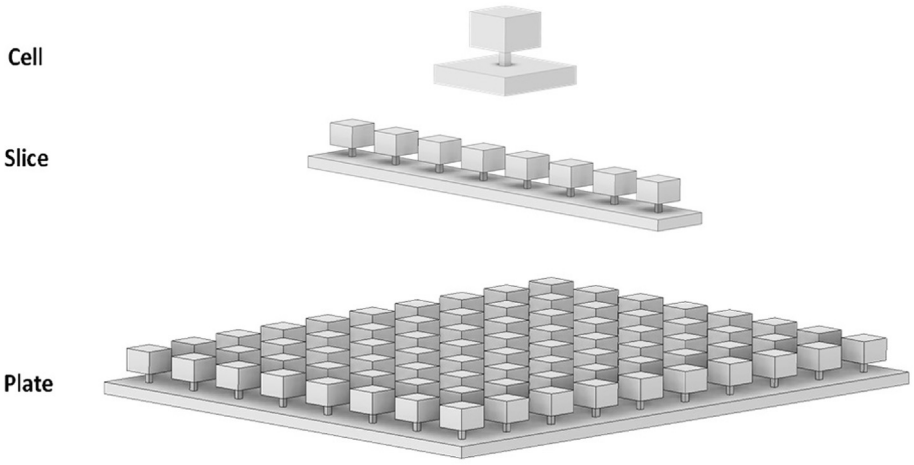

Fig. 10. The models of unit cell, slice and EM plate for FE and WFE simulations.

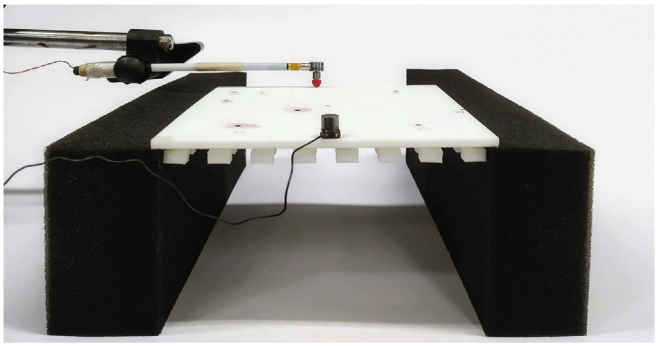

Fig. 11. Experimental setup with the 3D-printed EM plate.

Table 2
Measurement instrument specifications.

Instrument	Model	Sensitivity	Measure range
Hammer	PCB 86E80	23.11 mV/N	222.0 N (peak)
Accelerometer	KISTLER	3.86 mV/g	10 Hz–25 kHz
Data Acquisition	LMS SCR05	–	–

Table 3
3D-printed EM plate geometry and material properties.

Geometry/Property	Value
Lattice parameter (a)	0.012 m
Total length of the EM plate (L_t)	0.12 m
Total length of the resonator mass (L_m)	0.006 m
Total length of the resonator beam (L_b)	0.001 m
Unit cell area ($S = a^2$)	0.012×0.012 m^2
Cross section area of the EM plate ($S = b \times h$)	0.096×0.0028 m^2
Cross section area of resonator mass ($S_m = b_m \times h_m$)	0.006×0.0038 m^2
Cross section area of resonator beam ($S_b = b_b \times h_b$)	0.001×0.002 m^2
Young's modulus (E)	0.86×10^9 Pa
Mass density (ρ)	600 kg/m^3
Structural damping (η)	0.02
Poisson's ratio (ν)	0.39

Fabro et al., 2020). Another possible strategy is to perform a material characterisation procedure to derive the mechanical properties, for instance using static tests (Ye et al., 2020).

We also highlight that the first two resonant frequencies observed in Fig. 12, *i.e.*, 915.222 Hz and 917.343 Hz, match with the locally resonant band gap in Fig. 13 computed by FE and WFE approaches.

Fig. 14 compares the complex band structure calculated by PWE (real part of Bloch wave vector) and EPWE (for $\phi = 0°$) (imaginary part of Bloch wave vector), experimental (EXP) receptance and receptances computed by FE and WFE.

The Bloch wave vectors are obtained from PWE and EPWE presented in Subsections 2.1 and 2.2 from 0 Hz up to 2000 Hz. We consider an attached single resonator of S-DOF in the unit cell, regarding $f_1 = 915.222$ Hz (from modal analysis in Fig. 12(a)), material properties from Table 3 and 81 plane waves.

From PWE and EPWE results in Fig. 14, a locally resonant band gap opened up between 910 Hz and 1060 Hz can be observed. This result is in a good agreement with FE, WFE and experimental results. We highlight that the difference of the band gap width calculated by PWE/EPWE and FE/WFE is associated with PWE/EPWE modelling which does not consider the 3D geometry of the resonator. Thus, the modelling of the EM thick plate with attached spring-mass S-DOF resonators is capable to estimate the band gap width of an EM thick plate with 3D resonators obtained numerically and experimentally.

Fig. 15 shows the complex band structure computed by WFE for the unit cell modelled in ANSYS, thus the 3D geometry of the resonator is regarded. We highlight that only the first seven modes are plotted in Fig. 15.

Differently from the band structure calculated by PWE and EPWE (both considering only flexural modes) in Fig. 14, it is difficult to identify exactly the locally resonant band gap width in Fig. 15, since the band structure of a solid is more complex (Silva et al., 2016; Beli et al., 2018b). Accordingly, in order to facilitate the identification of the band gap width, we insert a rectangle in Fig. 15 using the same range of frequency of the locally resonant band gap width in the receptance of Fig. 13 for WFE, *i.e.*, from 870 Hz to 986 Hz. Furthermore, one can observe that the propagation of waves is strongly attenuated in these range of frequency.

5. Conclusions

An EM thick plate containing periodic resonators has been investigated in order to open up locally resonant and Bragg-type band gaps. We use PWE and EPWE methods to deal with the EM thick plate containing multiple resonators of S-DOF in the unit cell.

Complex band structures are calculated by PWE and EPWE using the Mindlin-Reissner plate theory in order to evaluate the EM thick plate performance in terms of band gap width and unit

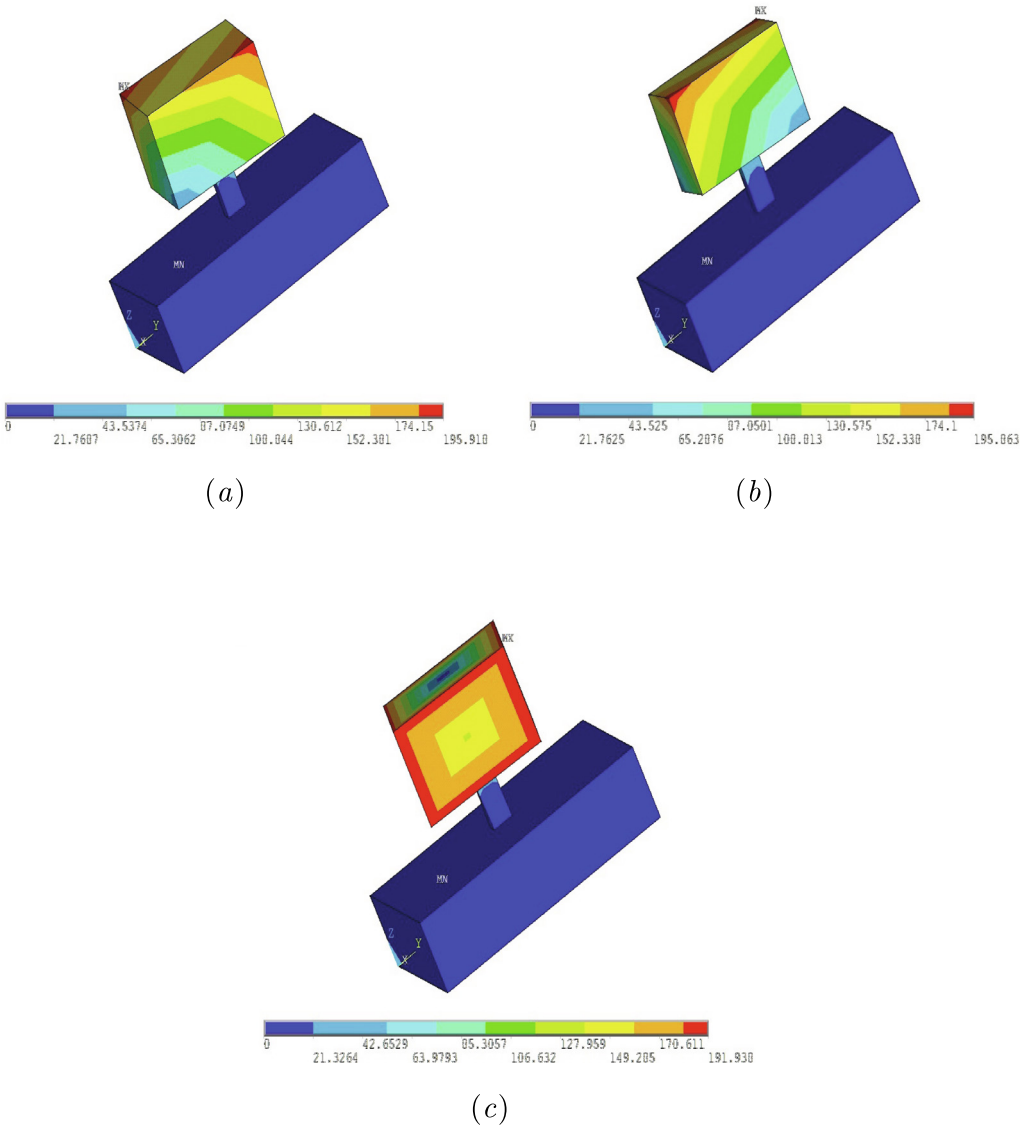

Fig. 12. Modal analysis of the unit cell using FE for a boundary condition of clamped on all edges (CCCC): (*a*) 915.222 Hz, (*b*) 917.343 Hz and (*c*) 1075.14 Hz.

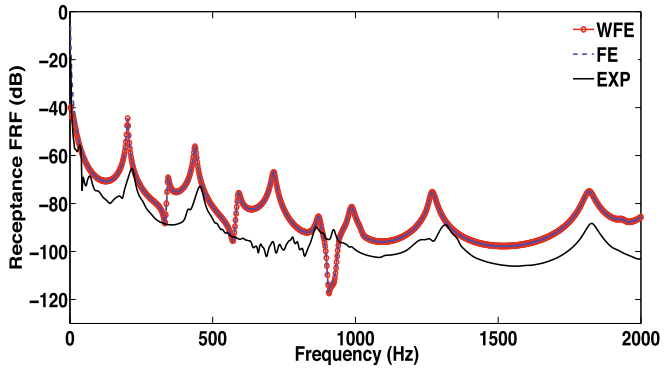

Fig. 13. Comparison of experimental (EXP) receptance and receptances computed by FE and WFE.

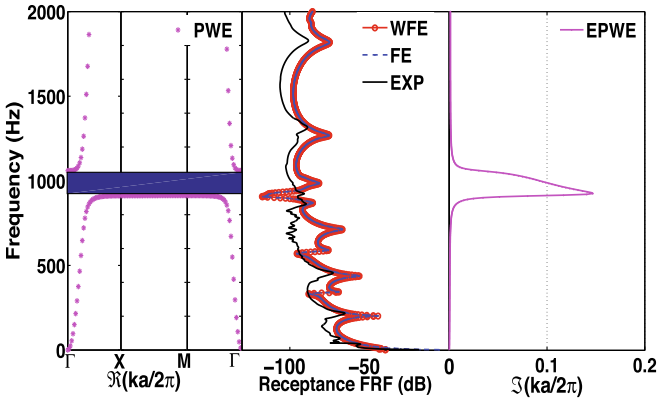

Fig. 14. Comparison of complex band structure calculated by PWE and EPWE (for $\phi = 0^{\circ}$), experimental (EXP) receptance and receptances computed by FE and WFE.

cell attenuation. A good agreement, at low frequencies, is observed between the complex band structures calculated by both Kirchhoff–Love and Mindlin-Reissner plate theories. The wave shapes are computed by using PWE. Depending on the type of band gap (Bragg-type or locally resonant) at the lower or upper edge frequency and on the configuration of the periodic arrays of attached

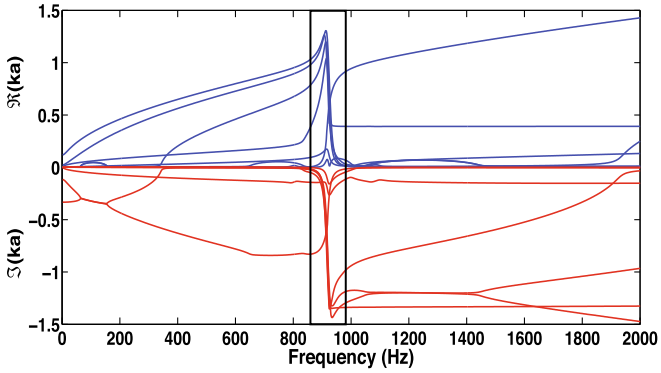

Fig. 15. Complex band structure computed by WFE.

resonators, the amplitude, symmetry and pattern of wave shapes are affected.

An experimental analysis was conducted with a 3D-printed EM plate with resonators. Modal analysis and forced response are computed by FE method. The WFE is used in order to obtain the complex band structure and the forced response. The PWE and EPWE approaches with spring-mass S-DOF resonators present a good agreement between FE and WFE modelling with 3D resonators and experimental results, in terms of band gap width.

The configuration of periodic arrays of attached resonators in thick plates enhances the possibility of using mechanical metamaterial plates for vibration attenuation.

Declaration of Competing Interest

The authors declare that they have no known competing financial interests or personal relationships that could have appeared to influence the work reported in this paper.

Acknowledgments

The authors gratefully acknowledge the support of the Brazilian funding agencies CAPES (Finance Code 001), CNPq (Grant Reference Number 313620/2018), FAPEMA and FAPESP (Grant Reference Number 2018/15894-0).

References

Achaoui, Y., Laude, V., Benchabane, S., Khelif, A., 2013. Local resonances in phononic crystals and in random arrangements of pillars on a surface. Journal of Applied Physics 114 (104503), 1–4. https://doi.org/10.1063/1.4820928.

Ampatzidis, T., Leach, R.K., Tuck, C.J., Chronopoulos, D., 2018. Band gap behaviour of optimal one-dimensional composite structures with an additive manufactured stiffener. Composites Part B 153, 26–35. https://doi.org/10.1016/j.compositesb.2018.07.012.

Assouar, B., Oudicha, M., Zhoua, X., 2016. Acoustic metamaterials for sound mitigation. Comptes Rendus Physique 17, 525–533. https://doi.org/10.1016/j.crhy.2016.02.002.

Bao, B., Wang, Q., 2019. Elastic wave manipulation in piezoelectric beam metastructure using electronic negative capacitance dual-adjacent/staggered connections. Composite Structures 210, 567–580. https://doi.org/10.1016/j.compstruct.2018.11.053.

Beli, D., Arruda, J.R.F., Ruzzene, M., 2018a. Wave propagation in elastic metamaterial beams and plates with interconnected resonators. International Journal of Solids and Structures 139–140, 105–120. https://doi.org/10.1016/j.ijsolstr.2018.01.027.

Beli, D., Mencik, J.-M., Silva, P.B., Arruda, J.R.F., 2018b. A projection-based model reduction strategy for the wave and vibration analysis of rotating periodic structures. Computational Mechanics 62 (6), 1511–1528. https://doi.org/10.1007/s00466-018-1576-7.

Beli, D., Fabro, A.T., Ruzzene, M., Arruda, J.R.F., 2019. Wave attenuation and trapping in 3D printed cantilever-in-mass metamaterials with spatially correlated variability. Scientific Reports 9 (5617), 1–11. https://doi.org/10.1038/s41598-019-41999-0.

Bertoldi, K., Vitelli, V., Christensen, J., van Hecke, M., 2017. Flexible mechanical metamaterials. Nature Reviews Materials 2 (17066), 1–11. https://doi.org/10.1038/natrevmats.2017.66.

Bilal, O.R., Foehr, A., Daraio, C., 2017. Observation of trampoline phenomena in 3D-printed metamaterial plates. Extreme Mechanics Letters 15, 103–107. https://doi.org/10.1016/j.eml.2017.06.004.

Bloch, F., 1928. Üdie quantenmechanik der electron in kristallgittern. Zeitschrift füysik 52, 555–600.

Brillouin, L., 1946. Wave Propagation in Periodic Structures. Dover Publications, New York.

Caliri Jr., M.F., Ferreira, A.J.M., Tita, V., 2016. A review on plate and shell theories for laminated and sandwich structures highlighting the Finite Element Method. Composite Structures 156, 63–77. doi: 10.1016/j.compstruct.2016.02.036. .

Carta, G., Colquitt, D.J., Movchan, A.B., Movchan, N.V., Jones, I.S., 2020. Chiral flexural waves in structured plates: directional localisation and control. Journal of the Mechanics and Physics of Solids 137 (103866), 1–16. https://doi.org/10.1016/j.jmps.2020.103866.

Casadei, F., Bertoldi, K., 2014. Wave propagation in beams with periodic arrays of airfoil-shaped resonating units. Journal of Sound and Vibration 333 (24), 6532–6547. https://doi.org/10.1016/j.jsv.2014.07.008.

Casadei, F., Dozio, L., Ruzzene, M., Cunefare, K.A., 2010. Periodic shunted arrays for the control of noise radiation in an enclosure. Journal of Sound and Vibration 329 (18), 3632–3646. https://doi.org/10.1016/j.jsv.2010.04.003.

Casadei, F., Beck, B.S., Cunefare, K.A., Ruzzene, M., 2012. Vibration control of plates through hybrid configurations of periodic piezoeletric shunts. Journal of Intelligent Material Systems and Structures 23 (10), 1169–1177. https://doi.org/10.1177/1045389X12443014.

Chen, Y., Huang, X., Sun, G., Yan, X., Li, G., 2014. Focusing and waveguiding of Lamb waves in micro-fabricated piezoelectric phononic plates. Ultrasonics 54, 1984–1990. https://doi.org/10.1016/j.compstruc.2017.01.001.

Chen, Y., Hu, G., Huang, G., 2017a. A hybrid elastic metamaterial with negative mass density and tunable bending stiffness. Journal of the Mechanics and Physics of Solids 105, 179–198. https://doi.org/10.1016/j.jmps.2017.05.009.

Chen, Y., Huang, X., Sun, G., Yan, X., Li, G., 2017b. Maximizing spatial decay of evanescent waves in phononic crystals by topology optimization. Computers and Structures 182, 430–447. https://doi.org/10.1016/j.compstruc.2017.01.001.

Cheng, Z.B., Shi, Z.F., Mo, Y.L., 2018. Complex dispersion relations and evanescent waves in periodic beams via the extended differential quadrature method. Composite Structures 187, 122–136. https://doi.org/10.1016/j.compstruct.2017.12.037.

Claeys, C.C., Vergote, K., Sas, P., Desmet, W., 2013. On the potential of tuned resonators to obtain low-frequency vibrational stop bands in periodic panels. Journal of Sound and Vibration 332, 1418–1436. https://doi.org/10.1016/j.jsv.2012.09.047.

Dal Poggetto, V.F., Arruda, J.R.F., 2021. Widening wave band gaps of periodic plates via shape optimization using spatial Fourier coefficients. Mechanical Systems and Signal Processing 147, . https://doi.org/10.1016/j.ymssp.2020.107098 107098.

Dal Poggetto, V.F., Serpa, A.L., 2020. Elastic wave band gaps in a three-dimensional periodic metamaterial using the plane wave expansion method. International Journal of Mechanical Sciences 184, . https://doi.org/10.1016/j.ijmecsci.2020.105841 105841.

Deng, J., Zheng, L., Guasch, O., Wu, H., Zeng, P., 2019. Gaussian expansion for the vibration analysis of plates with multiple acoustic black holes indentations. Mechanical Systems and Signal Processing 131, 317–334. https://doi.org/10.1016/j.ymssp.2019.05.024.

Dizona, J.R.C., Espera Jr., A.H., Chena, Q., Advincula, R.C., 2018. Mechanical characterization of 3D-printed polymers. Additive Manufacturing 20, 44–67. https://doi.org/10.1016/j.addma.2017.12.002.

Fabro, A.T., Meng, H., Chronopoulos, D., 2020. Uncertainties in the attenuation performance of a multi-frequency metastructure from additive manufacturing. Mechanical Systems and Signal Processing 138 (106557), 1–16. https://doi.org/10.1016/j.ymssp.2019.106557.

Fahy, F., Gardonio, P., 2007. Sound and Structural Vibration: Radiation, Transmission and Response. Academic Press.

Floquet, G., 1883. Sur les équations différentielles linéaires à coefficients périodiques. Annales scientifiques de l'École Normale Supérieure 12, 47–88.

Gao, N., Wu, J.H., Yu, L., 2015. Research on bandgaps in two-dimensional phononic crystal with two resonators. Ultrasonics 56, 287–293. https://doi.org/10.1016/j.ultras.2014.08.006.

Gao, N., Wu, J.H., Yu, L., 2016a. Low frequency band gaps below 10 Hz in radial flexible elastic metamaterial plate. Journal of Physics D: Applied Physics 49 (435501), 1–9. https://doi.org/10.1088/0022-3727/49/43/435501.

Gao, N., Wu, J.H., Yu, L., Xin, H., 2016b. Design of radial phononic crystal using annular soft material with low-frequency resonant elastic structures. Physics Letters A 380, 3326–3332. https://doi.org/10.1016/j.physleta.2016.08.010.

Han, X.K., Zhang, Z., 2019. Topological optimization of phononic crystal thin plate by a genetic algorithm. Scientific Reports 9, 8331. https://doi.org/10.1038/s41598-019-44850-8.

Hannon, R.J., 1975. Vibration and sound radiation of a plate. Journal of the Acoustical Society of America 58, S43. https://doi.org/10.1121/1.2002129.

Haslinger, S.G., Movchan, N.V., Movchan, A.B., Jones, I.S., Craster, R.V., 2017. Controlling flexural waves in semi-infinite platonic crystals with resonator-type scatterers. The Quarterly Journal of Mechanics and Applied Mathematics 70, 216–247. https://doi.org/10.1093/qjmam/hbx005.

Hedayatrasa, S., Kersemans, M., Abhary, K., Uddin, M., Paepegem, W.V., 2018. Optimization and experimental validation of stiff porous phononic plates for widest complete bandgap of mixed fundamental guided wave modes. Mechanical Systems and Signal Processing 98, 786–801. https://doi.org/10.1016/j.ymssp.2017.05.019.

He, Z.C., Xiao, X., Li, E., 2017. Design for structural vibration suppression in laminate acoustic metamaterials. Composites Part B: Engineering 131, 237–252. https://doi.org/10.1016/j.compositesb.2017.07.076.

Ho, K.M., Cheng, C.K., Yang, Z., Zhang, X.X., Sheng, P., 2003. Broadband locally resonant sonic shields. Applied Physics Letters 83 (26), 5566–5568. https://doi.org/10.1063/1.1637152.

Hsu, J.C., Wu, T.T., 2010. Plate waves in locally resonant sonic materials. Japanese Journal of Applied Physics 49 (07HB11), 1–5. https://doi.org/10.1143/JJAP.49.07HB11.

Hsue, Y.C., Freeman, A.J., 2005. Extended plane-wave expansion method in three-dimensional anisotropic photonic crystals. Physical Review B 72 (195118), 1–10. https://doi.org/10.1103/PhysRevB.72.195118.

Hsue, Y.C., Yang, T.J., 2004a. Contour of the attenuated length of an evanescent wave at constant frequency within a band gap of photonic crystal. Solid State Communications 129, 475–478. https://doi.org/10.1016/j.ssc.2003.11.023.

Hsue, Y.C., Yang, T.J., 2004b. Applying a modified plane-wave expansion method to the calculations of transmittivity and reflectivity of a semi-infinite photonic crystal. Physical Review E 70 (016706), 1–6. https://doi.org/10.1103/PhysRevE.70.016706.

Huang, J.K., Liu, X.W., Chen, X.H., Xiang, H.J., 2018. Multiple flexural-wave attenuation zones of periodic slabs with cross-like holes on an arbitrary oblique lattice: numerical and experimental investigation. Journal of Sound and Vibration 437, 135–149. https://doi.org/10.1016/j.jsv.2013.03.028.

Hu, G., Tang, L., Das, R., Gao, S., Liu, H., 2017. Acoustic metamaterials with coupled local resonators for broadband vibration suppression. AIP Advances 7 (025211), 1–13. https://doi.org/10.1063/1.4977559.

Hussein, M.I., Leamy, M.J., Ruzzene, M., 2014. Dynamics of phononic materials and structures: historical origins, recent progress, and future outlook. Applied Mechanics Reviews 66, (4) . https://doi.org/10.1115/1.4026911 040802.

Jung, J., Kim, H.G., Goo, S., Chang, K.J., Wang, S., 2019. Realisation of a locally resonant metamaterial on the automobile panel structure to reduce noise radiation. Mechanical Systems and Signal Processing 122, 206–231. https://doi.org/10.1016/j.ymssp.2018.11.050.

Kamotski, I.V., Smyshlyaev, V.P., 2019. Bandgaps in two-dimensional high-contrast periodic elastic beam lattice materials. Journal of the Mechanics and Physics of Solids 123, 292–304. https://doi.org/10.1016/j.jmps.2018.08.024.

Kirchhoff, G., 1850. Über das gleichgewicht und die bewegung einer elastischen scheibe. Journal für die reine and angewandtle Mathematik 40, 51–88.

Krushynska, A.O., Bosia, F., Miniaci, M., Pugno, N.M., 2017b. Spider web-structured labyrinthine acoustic metamaterials for low-frequency sound control. New Journal of Physics 19 (105001), 1–12. https://doi.org/10.1088/1367-2630/aa83f3.

Krushynska, A.O., Miniaci, M., Bosia, F., Pugno, N.M., 2017a. Coupling local resonance with Bragg band gaps in single-phase mechanical metamaterials. Extreme Mechanics Letters 12, 30–36. https://doi.org/10.1016/j.eml.2016.10.004.

Kushwaha, M.S., Halevi, P., Martínez, G., Dobrzynski, L., Djafari-Rouhani, B., 1994. Theory of acoustic band structure of periodic elastic composites. Physical Review B 49 (4), 2313–2322. https://doi.org/10.1103/PhysRevB.49.2313.

Laude, V., Achaoui, Y., Benchabane, S., Khelif, A., 2009. Evanescent Bloch waves and the complex band structure of phononic crystals. Physical Review B 80 (092301), 1–4. https://doi.org/10.1103/PhysRevB.80.092301.

Lee, G.-Y., Chong, C., Kevrekidis, P.G., Yang, J., 2016. Wave mixing in coupled phononic crystals via a variable stiffness mechanism. Journal of the Mechanics and Physics of Solids 95, 501–516. https://doi.org/10.1016/j.jmps.2016.06.005.

Li, Y., Zhu, L., Chen, T., 2017. Plate-type elastic metamaterials for low-frequency broadband elastic wave attenuation. Ultrasonics 73, 34–42. https://doi.org/10.1016/j.ultras.2016.08.019.

Li, S., Dou, Y., Chen, T., Wan, Z., Huang, J., Li, B., Zhang, F., 2019. Evidence for complete low-frequency vibration band gaps in a thick elastic steel metamaterial plate. Modern Physics Letters B 33 (4), 1950038. https://doi.org/10.1142/S0217984919500386.

Li, J., Yang, P., Li, S., 2020a. Phononic band gaps by inertial amplification mechanisms in periodic composite sandwich beam with lattice truss cores. Composite Structures 231 (111468), 1–13. https://doi.org/10.1016/j.compstruct.2019.111458.

Li, J., Fan, X., Li, F., 2020b. Numerical and experimental study of a sandwich-like metamaterial plate for vibration suppression. Composite Structures 238 (111969), 1–9. https://doi.org/10.1016/j.compstruct.2020.111969.

Liu, Y., Gao, L.t., 2007. Explicit dynamic finite element method for band-structure calculations of 2D phononic crystals. Solid State Communications 144, 89–93. https://doi.org/10.1016/j.ssc.2007.08.014.

Liu, Z., Zhang, X., Mao, Y., Zhu, Y.Y., Yang, Z., Chan, C.T., Sheng, P., 2000. Locally resonant sonic materials. Science 289 (5485), 1734–1736. https://doi.org/10.1126/science.289.5485.1734.

Liu, Y., Yu, D., Li, L., Zhao, H., Wen, J., Wen, X., 2007. Design guidelines for flexural wave attenuation of slender beams with local resonators. Physics Letters A 362 (5–6), 344–347. https://doi.org/10.1016/j.physleta.2006.10.056.

Liu, Z., Rumpler, R., Feng, L., 2018. Broadband locally resonant metamaterial sandwich plate for improved noise insulation in the coincidence region. Composite Structures 200, 165–172. https://doi.org/10.1016/j.compstruct.2018.05.033.

Lou, J., He, L., Yang, J., Kitipornchai, S., Wu, H., 2018. Wave propagation in viscoelastic phononic crystal rods with internal resonators. Applied Acoustics 141, 382–392.

Love, A.E.H., 1888. The small free vibrations and deformation of a thin elastic shell. Philosophical Transactions of the Royal Society 179, 491–546.

Lu, M.H., Feng, L., Chen, Y.F., 2009. Phononic crystals and acoustic metamaterials. Materials Today 12 (12), 34–42. https://doi.org/10.1016/S1369-7021(09)70315-3.

Lu, K., Wu, J.H., Jing, L., Gao, N., Guan, D., 2017. The two-degree-of-freedom local resonance elastic metamaterial plate with broadband low-frequency bandgaps. Journal of Physics D: Applied Physics 50, . https://doi.org/10.1088/1361-6463/50/9/095104 095104.

Lu, Z., Yu, X., Lau, S.K., Khoo, B.C., Cui, F., 2020. Membrane-type acoustic metamaterial with eccentric masses for broadband sound isolation. Applied Acoustics 157, . https://doi.org/10.1016/j.apacoust.2019.107003 107003.

Maldovan, M., 2013. Sound and heat revolutions in phononics. Nature 503, 209–217. https://doi.org/10.1038/nature12608.

Matlack, K.H., Bauhofer, A., Krödel, S., Palermo, A., Daraio, C., 2016. Composite 3D-printed metastructures for low-frequency and broadband vibration absorption. PNAS 113 (30), 8386–8390. https://doi.org/10.1073/pnas.1600171113.

McPhedran, R.C., Movchan, A.B., Movchan, N.V., Brun, M., Smith, M.J.A., 2018. 'Parabolic' trapped modes and steered Dirac cones in platonic crystals. Archive of Applied Mechanics 471, 20140746. https://doi.org/10.1098/rspa.2014.0746.

Mencik, J.-M., 2010. On the low- and mid-frequency forced response of elastic structures using wave finite elements with one-dimensional propagation. Computers and Structures 88, 674–689. https://doi.org/10.1016/j.compstruc.2010.02.006.

Mindlin, R.D., 1951. Thickness-shear and flexural vibrations of crystal plates. Journal of Applied Physics 22 (3), 316–323. https://doi.org/10.1063/1.1699948.

Miranda Jr., E.J.P., Dos Santos, J.M.C., 2019. Flexural wave band gaps in multi-resonator elastic metamaterial Timoshenko beams. Wave Motion 91, . https://doi.org/10.1016/j.wavemoti.2019.102391 102391.

Miranda Jr., E.J.P., Dos Santos, J.M.C., 2017. Flexural wave band gaps in phononic crystal Euler-Bernoulli beams using wave finite element and plane wave expansion methods. Materials Research 20 (Suppl. 2), 729–742. doi: 10.1590/1980-5373-MR-2016-0877. .

Miranda Jr., E.J.P., Dos Santos, J.M.C., 2018. Evanescent Bloch waves and complex band structure in magnetoelectroelastic phononic crystals. Mechanical Systems and Signal Processing 112, 280–304. doi: 10.1016/j.ymssp.2018.04.034. .

Miranda Jr., E.J.P., Nobrega, E.D., Ferreira, A.H.R., Dos Santos, J.M.C., 2019. Flexural wave band gaps in a multi-resonator elastic metamaterial plate using Kirchhoff-Love theory. Mechanical Systems and Signal Processing 116, 480–504. doi: 10.1016/j.ymssp.2018.06.059. .

Morvaridi, M., Carta, G., Brun, M., 2018. Platonic crystal with low-frequency locally-resonant spiral structures: wave trapping, transmission amplification, shielding and edge waves. Journal of the Mechanics and Physics of Solids 121, 496–516. https://doi.org/10.1016/j.jmps.2018.08.017.

Movchan, A.B., McPhedran, R.C., Carta, G., Craster, R.V., 2018. Platonic localisation: one ring to bind them. Archive of Applied Mechanics 89, 521–533. https://doi.org/10.1007/s00419-018-1465-8.

Ngo, T.D., Kashani, A., Imbalzano, G., Nguyen, K.T.Q., Hui, D., 2018. Additive manufacturing (3D printing): a review of materials, methods, applications and challenges. Composites Part B 143, 172–196. https://doi.org/10.1016/j.compositesb.2018.02.012.

Nobrega, E.D., Gautier, F., Pelat, A., Dos Santos, J.M.C., 2016. Vibration band gaps for elastic metamaterial rods using wave finite element method. Mechanical Systems and Signal Processing 79, 192–202. https://doi.org/10.1016/j.ymssp.2016.02.059.

Oudich, M., Senesi, M., Assouar, M.B., Ruzenne, M., Sun, J.H., Vincent, B., Hou, Z., Wu, T.T., 2011. Experimental evidence of locally resonant sonic band gap in two-dimensional phononic stubbed plates. Physical Review B 84 (165136), 1–6. https://doi.org/10.1103/PhysRevB.84.165136.

Oudich, M., Zhou, X., Assouar, M.B., 2014. General analytical approach for sound transmission loss analysis through a thick metamaterial plate. Journal of Applied Physics 116, . https://doi.org/10.1063/1.4901997 193509.

Pal, R.K., Ruzzene, M., 2017. Edge waves in plates with resonators: an elastic analogue of the quantum valley Hall effect. New Journal of Physics 19 (025001), 517–528. https://doi.org/10.1088/1367-2630/aa56a2.

Peng, H., Pai, P.F., Deng, H., 2015. Acoustic multi-stopband metamaterial plates design for broadband elastic wave absorption and vibration suppression. International Journal of Mechanical Sciences 103, 104–114. https://doi.org/10.1016/j.ijmecsci.2015.08.024.

Pennec, Y., Vasseur, J.O., Djafari-Rouhani, B., Dobrzyński, L., Deymier, P.A., 2010. Two-dimensional phononic crystals: examples and applications. Surface Science Reports 65 (8), 229–291. https://doi.org/10.1016/j.surfrep.2010.08.002.

Qian, D., 2020. Electro-mechanical coupling wave propagating in a locally resonant piezoelectric/elastic phononic crystal nanobeam with surface effects. Applied Mathematics and Mechanics 41, 425–438. https://doi.org/10.1007/s10483-020-2586-5.

Qian, D., Shi, Z., 2016. Bandgap properties in locally resonant phononic crystal double panel structures with periodically attached spring-mass resonators. Physics Letters A 380, 3319–3325. https://doi.org/10.1016/j.physleta.2016.07.068.

Qian, D., Shi, Z., 2017. Using PWE/FE method to calculate the band structures of the semi-infinite beam-like PCs: periodic in z-direction and finite in x-y plane. Physics Letters A 381, 1516–1524. https://doi.org/10.1016/j.physleta.2017.02.049.

Raghavan, L., Phani, A.S., 2013. Local resonance bandgaps in periodic media: theory and experiment. Journal of Acoustical Society of America 134 (3), 1950–1959. https://doi.org/10.1121/1.4817894.

Romero-García, V., Sánchez-Pérez, J.V., Castiñeira-Ibáñez, S., Garcia-Raffi, L.M., 2010a. Evidences of evanescent Bloch waves in phononic crystals. Applied Physics Letters 96 (124102), 1–3. https://doi.org/10.1063/1.3367739.

Romero-García, V., Sánchez-Pérez, J.V., Garcia-Raffi, L.M., 2010b. Evanescent modes in sonic crystals: complex dispersion relation and supercell approximation. Journal of Applied Physics 108 (044907), 1–6. https://doi.org/10.1063/1.3466988.

Romero-García, V., Sánchez-Pérez, J.V., Garcia-Raffi, L.M., 2010c. Propagating and evanescent properties of double-point defects in sonic crystals. New Journal of Physics 12 (083024), 1–14. https://doi.org/10.1088/1367-2630/12/8/083024.

Sigalas, M.M., Economou, E.N., 1992. Elastic and acoustic wave band structure. Journal of Sound and Vibration 158 (2), 377–382. https://doi.org/10.1016/0022-460X(92)90059-7.

Silva, P.B., Mencik, J.-M., Arruda, J.R.F., 2016. On the use of the wave finite element method for passive vibration control of periodic structures. Advances in Aircraft and Spacecraft Science 3 (3), 299–315. https://doi.org/10.12989/aas.2016.3.3.299.

Song, Y., Feng, L., Wen, J., Yu, D., Wen, X., 2015. Analysis and enhancement of flexural wave stop bands in 2D periodic plates. Physics Letters A 379, 1449–1456. https://doi.org/10.1016/j.physleta.2015.01.037.

Sugino, C., Xia, Y., Leadenham, S., Ruzzene, M., Erturk, A., 2017. A general theory for bandgap estimation in locally resonant metastructures. Journal of Sound and Vibration 406, 104–123. https://doi.org/10.1016/j.jsv.2017.06.004.

Sugino, C., Ruzzene, M., Erturk, A., 2018. Merging mechanical and electromechanical bandgaps in locally resonant metamaterials and metastructures. Journal of the Mechanics and Physics of Solids 116, 323–333. https://doi.org/10.1016/j.jmps.2018.04.005.

Sugino, C., Ruzzene, M., Erturk, A., 2020. An analytical framework for locally resonant piezoelectric metamaterial plates. International Journal of Solids and Structures 182–183, 281–294. https://doi.org/10.1016/j.ijsolstr.2019.08.011.

Sun, C.Y., Hsu, J.C., Wu, T.T., 2010. Resonant slow modes in phononic crystal plates with periodic membranes. Applied Physics Letters 97 (031902), 1–3. https://doi.org/10.1063/1.3464955.

Surjadi, J.U., Gao, L., Du, H., Li, X., Xiong, X., Fang, N.X., Lu, Y., 2019. Mechanical metamaterials and their engineering applications. Advanced Engineering Materials 21 (3), 1800864. https://doi.org/10.1002/adem.201800864.

Thorp, O., Ruzzene, M., Baz, A., 2005. Attenuation of wave propagation in fluid-loaded shells with periodic shunted piezoeletric rings. Smart Materials and Structures 14, 594–604. https://doi.org/10.1088/0964-1726/14/4/018.

Torrent, D., Mayou, D., Sánchez-Dehesa, J., 2013. Elastic analog of graphene: Dirac cones and edge states for flexural waves in thin plates. Physical Review B 87 (115143), 1–8. https://doi.org/10.1103/PhysRevB.87.115143.

Wang, M.Y., Wang, X., 2013. Frequency band structure of locally resonant periodic flexural beams suspended with force-moment resonators. Journal of Physics D: Applied Physics 46 (255502), 1–8. https://doi.org/10.1088/0022-3727/46/25/255502.

Wang, G., Wen, X., Wen, J., Liu, Y., 2005a. Quasi-one-dimensional periodic structure with locally resonant band gap. Journal of Applied Mechanics 73 (1), 167–170. https://doi.org/10.1115/1.2061947.

Wang, G., Wen, J., Wen, X., 2005b. Quasi-one-dimensional phononic crystals studied using the improved lumped-mass method: Application to locally resonant beams with flexural wave band gap. Physical Review B 71 (104302), 1–5. https://doi.org/10.1103/PhysRevB.71.104302.

Wang, Z., Zhang, P., Zhang, Y., 2013. Locally resonant band gaps in flexural vibrations of a Timoshenko beam with periodically attached multioscillators. Mathematical Problems in Engineering 2013 (146975), 1–10. https://doi.org/10.1155/2013/146975.

Wang, M.Y., Choy, Y.T., Wan, C.W., Zhao, A.S., 2015. Wide band-gaps in flexural periodic beams with separated force and moment resonators. Journal of Vibration and Acoustics 137 (6), 1–6. https://doi.org/10.1115/1.4031519.

Wang, T., Sheng, M.P., Qin, Q.H., 2016. Multi-flexural band gaps in an Euler-Bernoulli beam with lateral local resonators. Physics Letters A 380 (4), 525–529. https://doi.org/10.1016/j.physleta.2015.12.010.

Wang, X., Jiang, M., Zhou, Z., Gou, J., Hui, D., 2017. 3D printing of polymer matrix composites: a review and prospective. Composites Part B 110, 442–458. https://doi.org/10.1016/j.compositesb.2016.11.034.

Wang, K., Zhou, J., Cai, C., Xu, D., Ouyang, H., 2019. Mathematical modeling and analysis of a meta-plate for very low-frequency band gap. Applied Mathematical Modelling 73, 581–597. https://doi.org/10.1016/j.apm.2019.04.033.

Wu, Y., Yu, K., Yang, L., Zhao, R., Shi, X., 2018. Effect of thermal stresses on frequency band structures of elastic metamaterial plates. Journal of Sound and Vibration 413, 101–119. https://doi.org/10.1016/j.jsv.2017.10.014.

Wu, Z., Liu, W., Li, F., Zhang, C., 2019. Band-gap property of a novel elastic metamaterial beam with X-shaped local resonators. Mechanical Systems and Signal Processing 134, . https://doi.org/10.1016/j.ymssp.2019.106357 106357.

Xiao, Y., Wen, J., Wen, X., 2012a. Sound transmission loss of metamaterial-based thin plates with multiple subwavelength arrays of attached resonators. Journal of Sound and Vibration 331 (25), 5408–5423. https://doi.org/10.1016/j.jsv.2012.07.016.

Xiao, Y., Wen, J., Wen, X., 2012b. Longitudinal wave band gaps in metamaterial-based elastic rods containing multi-degree-of-freedom resonators. New Journal of Physics 14 (033042), 1–20. https://doi.org/10.1088/1367-2630/14/3/033042.

Xiao, Y., Wen, J., Wen, X., 2012c. Broadband locally resonant beams containing multiple periodic arrays of attached resonators. Physics Letters A 376 (16), 1384–1390. https://doi.org/10.1016/j.physleta.2012.02.059.

Xiao, Y., Wen, J., Wen, X., 2012d. Flexural wave band gaps in locally resonant thin plates with periodically attached spring-mass resonators. Journal of Physics D: Applied Physics 45 (19), 1–12. https://doi.org/10.1088/0022-3727/45/19/195401.

Xiao, Y., Wen, J., Yu, D., Wen, X., 2013. Flexural wave propagation in beams with periodically attached vibration absorbers: band-gap behavior and band formation mechanisms. Journal of Sound and Vibration 332 (4), 867–893. https://doi.org/10.1016/j.jsv.2012.09.035.

Xiao, Y., Wen, J., Huang, L., Wen, X., 2014. Analysis and experimental realization of locally resonant phononic plates carrying a periodic array of beam-like resonators. Journal of Physics D: Applied Physics 47 (045307), 12pp. doi: 10.1088/0022-3727/47/4/045307. .

Xiao, X., He, Z.C., Li, E., Cheng, A.G., 2019. Design multi-stopband laminate acoustic metamaterials for structural-acoustic coupled system. Mechanical Systems and Signal Processing 115, 418–433. https://doi.org/10.1016/j.ymssp.2018.06.004.

Xie, L., Xia, B., Liu, J., Huang, G., Lei, J., 2017. An improved fast plane wave expansion method for topology optimization of phononic crystals. International Journal of Mechanical Sciences 120, 171–181. https://doi.org/10.1016/j.ijmecsci.2016.11.023.

Yang, Z., Dai, H.M., Chan, N.H., Ma, G.C., 2010. Acoustic metamaterial panels for sound attenuation in the 50–1000 Hz regime. Applied Physics Letters 96 (041906), 1–3. https://doi.org/10.1063/1.3299007.

Yang, J., Lee, J.S., Kim, Y.Y., 2015. Metaporous layer to overcome the thickness constraint for broadband sound absorption. Journal of Applied Physics 117, (17) . https://doi.org/10.1063/1.4919844 174903.

Yao, Z.J., Yu, G.L., Wang, Y.S., Shi, Z.F., 2009. Propagation of bending waves in phononic crystal thin plates with a point defect. International Journal of Solids and Structures 46 (13), 2571–2576. https://doi.org/10.1016/j.ijsolstr.2009.02.002.

Ye, M., Gao, L., Li, H., 2020. A design framework for gradually stiffer mechanical metamaterial induced by negative Poisson's ratio property. Materials and Design 192, . https://doi.org/10.1016/j.matdes.2020.108751 108751.

Yu, D., Liu, Y., Wang, G., Zhao, H., Qiu, J., 2006a. Flexural vibration band gaps in Timoshenko beams with locally resonant structures. Journal of Applied Physics 100 (124901), 1–5. https://doi.org/10.1063/1.2400803.

Yu, D., Liu, Y., Zhao, H., Wang, G., Qiu, J., 2006b. Flexural vibration band gaps in Euler-Bernoulli beams with locally resonant structures with two degrees of freedom. Physical Review B 73 (064301), 1–5. https://doi.org/10.1103/PhysRevB.73.064301.

Yu, K., Chen, T., Wang, X., 2013. Band gaps in the low-frequency range based on the two-dimensional phononic crystals plates composed of rubber matrix with periodic steel stubs. Physica B: Condensed Matter 416, 12–16. https://doi.org/10.1016/j.physb.2013.02.011.

Yu, D.-L., Du, C.-Y., Shen, H.-J., Liu, J.-W., Wen, J.-H., 2017. An analysis of structural-acoustic coupling band gaps in a fluid-filled periodic pipe. Chinese Physics Letters 34 (7), 076202–076206. https://doi.org/10.1088/0256-307X/34/7/076202.

Yu, X., Zhou, J., Liang, H., Jiang, Z., Wu, L., 2018. Mechanical metamaterials associated with stiffness, rigidity and compressibility: a brief review. Progress in Materials Science 94, 114–173. https://doi.org/10.1016/j.pmatsci.2017.12.003.

Zhang, G.Y., Gao, X.-L., 2018. Elastic wave propagation in 3-D periodic composites: band gaps incorporating microstructure effects. Composite Structures 204, 920–932. https://doi.org/10.1016/j.compstruct.2018.07.115.

Zhang, K., Zhao, P., Zhao, C., Hong, F., Deng, Z., 2020. Study on the mechanism of band gap and directional wave propagation of the auxetic chiral lattices. Composite Structures 238 (111952), 1–13. https://doi.org/10.1016/j.compstruct.2020.111952.

Zouari, S., Brocail, J., Génevaux, J.M., 2018. Flexural wave band gaps in metamaterial plates: a numerical and experimental study from infinite to finite models. Journal of Sound and Vibration 435, 246–263. https://doi.org/10.1016/j.jsv.2018.07.030.

Zuo, S., Huang, H., Wu, X., Zhang, M., Ni, T., 2018. Low-frequency band gap of locally resonant phononic crystals with a dual-base plate. The Journal of the Acoustical Society of America 143 (3), 1326–1332. https://doi.org/10.1121/1.5025041.